TABLE 1

Effects of nAChR antagonists and agonists on C4 respiratory rate

Drug	Concentration (μM)	n	C4 respiratory rate (min^{-1})		
			Control	Drug (% of control)	Washout
Meca	0.1	7	5.5±0.3	4.5±0.3* (81.4±3.0)	5.3±0.3
	1	7	5.4±0.3	4.0±0.3** (73.0±2.7)	4.9±0.3
	10	7	5.3±0.3	3.5±0.5*** (65.0±4.7)	4.8±0.3
	100	7	5.6±0.4	3.5±0.4*** (61.4±3.2)	4.3±0.6
DH-β-E	0.1	7	6.8±0.7	5.6±0.7** (82.3±3.2)	6.4±0.7
	1	7	6.7±0.6	5.1±0.7*** (74.5±4.3)	6.2±0.7
	10	7	6.7±0.8	4.4±0.8** (62.0±6.6)	6.1±0.8
	100	7	7.3±0.7	4.0±0.8*** (51.6±6.4)	4.9±0.4
MLA	0.1	7	6.1±0.7	4.8±0.7** (77.2±2.8)	5.6±0.7
	1	7	6.2±0.7	4.4±0.8*** (66.9±5.3)	5.8±0.6
	10	7	6.3±0.8	3.6±0.8*** (52.7±5.8)	5.5±0.8
	100	7	6.1±0.8	3.0±0.8*** (44.1±6.5)	5.5±0.8
α-BgTx	0.01	6	6.1±0.4	5.2±0.5** (84.4±3.0)	5.9±0.4
	0.1	6	6.4±0.4	4.8±0.3*** (74.8±2.2)	6.1±0.4
	1	6	6.9±0.6	4.8±0.5*** (69.1±3.1)	5.9±0.5
RJR	0.1	7	4.8±0.8	5.3±0.6*** (110.3±1.9)	4.9±0.9
	1	7	5.0±0.6	6.2±0.7** (122.3±3.5)	5.3±0.6
	10	7	5.2±0.4	10.6±1.3** (202.8±12.7)	6.1±0.3

Meca: mecamylamine; DH-β-E: dihydro-β-erythroidine; MLA: methyllycaconitine; a-BgTx: a-bungarotoxin; RJR: RJR-2403
*$P<0.05$
**$P<0.01$
***$P<0.001$

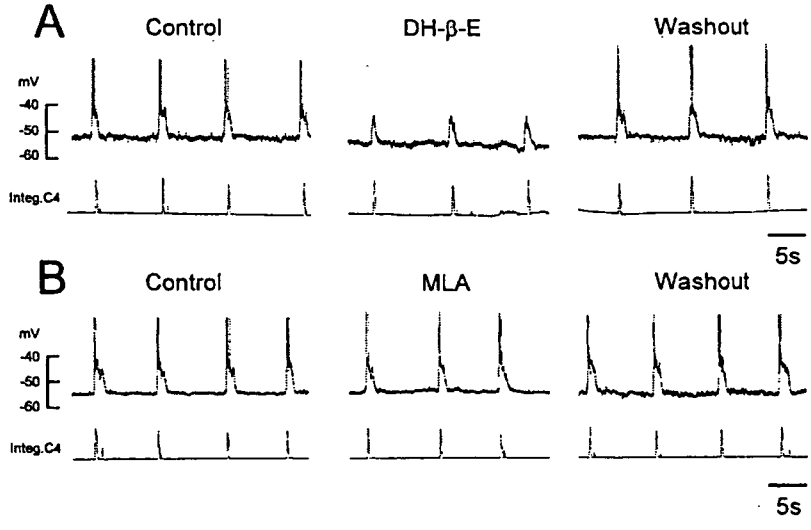

Figure 2: Effects of DH-β-E (A) and MLA (B) on the activity of inspiratory neurons. Top traces show the membrane potential of inspiratory neurons before (Control), during (DH-β-E 20μM or MLA 20μM), and after the application of DH-β-E and MLA. Bottom traces show integrated C4 (Integ.C4) activity (Washout).

TABLE 2.

Effects of DH-β-E and MLA on inspiratory neuron and C4 respiratory rate

	DH-β-E 20μM (n = 6)			MLA 20μM (n = 6)		
	Control	DH-β-E	Washout	Control	MLA	Washout
C4 respiratory rate (min^{-1})	5.8±0.8	3.6±0.6***	5.2±0.7	5.1±0.5	3.1±0.5***	4.9±0.5
Depolarizing cycle rate (min^{-1})	5.8±0.8	3.6±0.6***	5.2±0.7	5.1±0.5	3.1±0.5***	4.9±0.5
Intraburst firing frequency (Hz)	16.1±3.6	10.4±2.7**	15.0±3.3	11.4±2.2	10.9±2.2*	11.2±2.3
E_m (mV)	-53.9±0.6	-59.1±1.0***	-55.1±1.0	-55.5±0.7	-55.6±0.7	-55.7±0.8
Drive potential duration (s)	1.9±0.2	1.3±0.1***	1.8±0.2	1.6 ± 0.1	1.6±0.1	1.6±0.1
Drive potential amplitude (mV)	9.6±1.3	7.4±0.7*	9.0±1.2	9.4±1.3	9.2±1.2	9.2±1.2

DH-β-E: dihydro-β-erythroidine; MLA: methyllycaconitine; E_m: membrane potential
*$P<0.05$
**$P<0.01$
***$P<0.001$

Effects of DH-β-E and MLA on Pre-I neurons

Both DH-β-E and MLA decreased C4 respiratory rate and depolarizing cycle rate and induced significant hyperpolarization of E_m and reduction of intraburst firing frequency (Fig. 3; Table 3).

DISCUSSION

The present study has shown that α4β2 nAChR antagonist DH-β-E and α7 nAChR antagonists MLA and α-BgTx decrease C4 respiratory rate in a dose-dependent fashion, while the α4β2 nAChR agonist RJR induces dose-dependent increases in C4 respiratory rate. These results indicate that both α4β2 and α7 nAChR subtypes participate in the regulation of respiratory activity in preparations of neonatal rat brainstem-spinal cord.

In addition, we have shown that the α4β2 nAChR antagonist DH-β-E induces hyperpolarization of E_m and decreases in intraburst firing frequency in both Insp and Pre-I neurons. The α7 nAChR antagonist MLA, however, has distinct effects on each of the major respiratory neuron populations: in Insp neurons, MLA does not affect E_m polarity, but causes decreased intraburst firing frequency, while in pre-I neurons, it induces hyperpolarization of E_m and decreased intraburst firing frequency. These results indicate that in brainstem-spinal cord preparation of neonatal rat, the α4β2 nAChR subunit participates in the regulation of Insp neuronal activity, while both the α4β2 and α7 nAChR subunits are present in Pre-I neurons and cooperate to modulate C4 respiratory rate.

In the brainstem-spinal cord preparation used in this study, ACh produces increases in C4 respiratory rate that can be blocked partially by atropine, a muscarinic ACh receptor antagonist (Murakoshi et al., 1985).

In this same preparation, the application of DH-β-E has no effect on ACh-induced increases in C4 respiratory rate, but the additional application of atropine completely blocks ACh-induced response (Murakoshi et al., 1985). Moreover, Meca has no effect on ACh-induced increases in C4 respiratory rate and the sole application of gallamine, a NMBA, also shows no effect on C4 respiratory rate (Monteau et al., 1990). Taken together, these previous studies have suggested that nAChRs are not involved directly in central respiratory control of brainstem-spinal cord preparation from neonatal rats, in which muscarinic ACh receptors play the dominant role, and

that the contribution of cholinergic mechanisms to respiratory rhythm generation at rest is slight. However, our previous work has demonstrated that the sole application of NMBAs, which function as muscular nAChR antagonists, induces dose-dependent reductions in C4 respiratory rate (Sakuraba et al., 2003) and respiratory CO_2 responsiveness (Sakuraba et al., 2005). It also has been shown that respiratory CO_2 responsiveness is partly inhibited by the sole application of Meca and DH-β-E in the isolated brainstem-spinal cord preparation of neonatal rat (Kuwana et al., 2000). These findings strongly suggest that central respiratory control, including chemosensitivity, is directly mediated by nAChRs in the isolated brainstem-spinal cord preparation of neonatal rats.

nAChRs are expressed in the RVLM, which has been identified as a locus of central respiratory control. These receptors are made up of two functional subunits, α4β2 and α7 (Wada et al., 1989; Dominguez del Toro et al., 1994). In a previous study, NMBAs were shown to inhibit neuronal α4β2 and α7 nAChRs expressed in *Xenopus* oocyte, which was interesting in that NMBAs are known to be antagonists of muscular nAChR (Chiodini et al., 2001). Given these and our previous results (Sakuraba et al., 2003, 2005), we hypothesized that both the α4β2 and α7 nAChRs are involved directly in central respiratory control. And, in fact, we found that the sole administration of Meca, DH-β-E, MLA, and α-BgTx decrease C4 respiratory rate and that RJR increases C4 respiratory rate in the isolated brainstem-spinal cord preparation of neonatal rats.

In previous studies using medullary slice preparations from neonatal rats, nicotine-induced increases of respiratory frequency are completely blocked by Meca (Shao and Feldman, 2001), hexamethonium (Shao and Feldman, 2002), and DH-β-E (Shao and Feldman, 2002), but are not blocked by MLA or α-BgTx (Shao and Feldman, 2002). It also was reported that RJR increases respiratory frequency in a medullary slice preparation (Shao and Feldman, 2002).

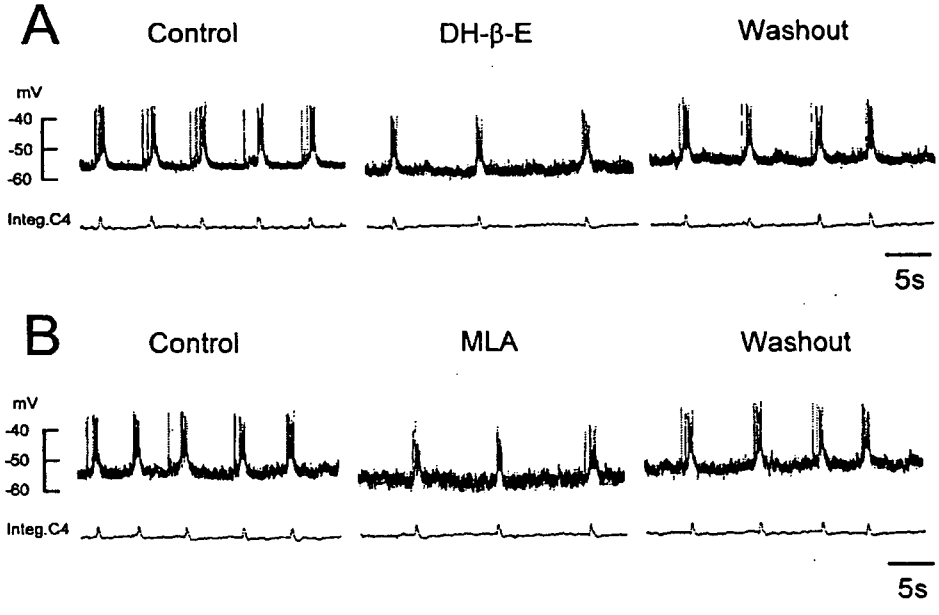

Figure 3: Effects of DH-β-E (A) and MLA (B) on the activity of preinspiratory neurons. Top traces show the membrane potential of preinspiratory neurons before (Control), during (DH-β-E 20μM or MLA 20μM), and after the application of DH-β-E and MLA. Bottom traces show integrated C4 (Integ.C4) activity (Washout).

TABLE 3

Effects of DH-β-E and MLA on preinspiratory neuron and C4 respiratory rate

	DH-β-E 20μM (n = 6)			MLA 20μM (n = 6)		
	Control	DH-β-E	Washout	Control	MLA	Washout
C4 respiratory rate (min^{-1})	4.7±0.8	2.8±0.5**	4.6±0.8	4.5±0.6	2.9±0.5***	4.3±0.6
Depolarizing cycle rate (min^{-1})	4.7±0.8	2.8±0.5**	4.6±0.8	4.5±0.6	2.9±0.5***	4.3±0.6
Intraburst firing frequency (Hz)	7.1±1.1	4.3±0.9***	6.8±1.0	7.1±0.8	3.6±0.6***	6.6±0.7
E_m (mV)	-57.7±1.8	-61.1±1.5**	-57.6±2.0	-57.4±1.6	-60.9±1.3***	-57.7±1.5

DH-β-E: dihydro-β-erythroidine; MLA: methyllycaconitine; E_m: membrane potential
*$P<0.05$
**$P<0.01$
***$P<0.001$

These past studies indicated that respiratory frequency is modulated by α4β2, but not by α7 nAChR, at least in medullary slice preparations from neonatal rats. This, however, is not consistent with our results in which both α4β2 and α7 nAChR are shown to contribute to central respiratory control. Pre-I neurons are absent in medullary slice preparations, but present in isolated brainstem-spinal cord preparations of neonatal rats, a difference that prompted us to study the effects of DH-β-E and MLA on Pre-I neurons and Insp neurons.

Pre-I neurons play a crucial role in the generation of respiratory rhythm (Onimaru et al., 1988; Onimaru et al., 1989; Onimaru et al., 1997; Onimaru and Homma, 2003) and the determination of motoneuron burst timing (Mellen et al., 2003; Sakuraba et al., 2003) in brainstem-spinal cord preparations of neonatal rats. However, the role of nAChRs in respiratory neurons has been investigated only in medullary slice preparation of neonatal rats, in which the Pre-I neurons are absent. In these slice preparations, a low concentration of nicotine induces a tonic inward current and increases in the frequency and amplitude of spontaneous excitatory postsynaptic current in preBötzinger Complex Insp neurons (Shao and Feldman, 2002). These nicotine-induced effects on preBötzinger Complex Insp neurons can be reversed by DH-β-E and are unaffected by MLA or α-BgTx (Shao and Feldman, 2002). The authors of that study concluded that α4β2 nAChRs modulate respiratory pattern via preBötzinger Complex Insp neurons. This is certainly consistent with our findings that DH-β-E has an inhibitory effect on Insp neurons, i.e. hyperpolarization of E_m, and causes reductions in intraburst firing frequency, drive potential duration, and drive potential amplitude. However, we also found that DH-β-E induces hyperpolarization of E_m and a reduction in intraburst firing frequency in Pre-I neurons. These findings strongly suggest that α4β2 nAChRs are located in both Insp and Pre-I neurons, where they serve to modulate central respiratory activities.

We have further shown that MLA also induces hyperpolarization of E_m and reductions in intraburst firing frequency in Pre-I neurons. And although it decreases intraburst firing frequency in Insp neurons, MLA does not affect their E_m, drive potential duration or drive potential amplitude. It has been shown that Insp neurons receive excitatory synaptic connections from Pre-I neurons (Onimaru et al., 1992, 1996, 1997; Ballanyi et al., 1999; Takeda et al., 2001). Taking this mechanism into account, we speculate that MLA mainly exerts its inhibitory effect on Pre-I, but not Insp, neurons, thereby reducing the excitatory drive from Pre-I neurons to Insp neurons and lowering the intraburst firing frequency of Insp neurons as an indirect result.

Furthermore, α7 nAChRs are expressed in presynaptic terminal and mediate Ca^{2+} entry via voltage-sensitive Ca^{2+} channels, and α7 nAChRs themselves are high permeable of Ca^{2+} for the release of ACh in the central nervous system (McGehee et al., 1995; Gray et al., 1996; Wonnacott, 1997). In the brainstem-spinal cord preparation, voltage-sensitive Ca^{2+} channels are related to the initiation and termination of hyperpolarization and depolarization of Pre-I neurons (Onimaru et al., 1996). Therefore, we can speculate that α7 nAChRs in Pre-I neurons partly characterize the Pre-I neuron burst and affect the respiratory rhythm.

In contrast to our previous study (Sakuraba et al., 2003), neither DH-β-E nor MLA induce a desynchronization of C4 respiratory rate and depolarizing cycle rate of Pre-I neurons during drug-induced respiratory depression. However, the NMBA used in the previous study was a muscular nAChR antagonist, not a pure neuronal nAChR antagonist, and we have not analyzed how these drugs might suppress central respiratory activity. It would be interesting to study this question by simultaneous bath application of DH-β-E and MLA in a future study. Further studies also are needed to analyze the different effects of NMBAs and neuronal nAChR antagonists on the desynchronization of C4 respiratory rate and depolarizing cycle rate in Pre-I neurons.

Ca^{2+} entry through neuronal nAChR modulates many biological processors in nervous tissue, and their permeability through α4β2 and α7 nAChRs are different (Fucile et al., 2005). Nevertheless, in our study, the responses of C4 and Pre-I neuron activities induced by the effects of MLA and DH-β-E are not different. Therefore, further studies are needed to analyze the relationship between neuronal nAChR-induced Ca^{2+} permeability change and respiratory activity.

In conclusion, both α4β2 and α7 nAChR subunits are involved in central respiratory control in brainstem-spinal cord preparations from neonatal rats, and α4β2 nAChRs function in both Pre-I and Insp neurons, while α7 nAChRs function solely in Pre-I neurons.

ACKNOWLEDGEMENTS

This work was supported in part by the Keio Gijuku Postgraduate School Fund for the Advancement of Research (S.S.), the Keio University Grant-in-Aid for Encouragement of Young Medical Scientists (S.S.), the Smoking Research Foundation (S.K.), and the Grant-in-Aid for Scientific Research from the Japanese Ministry of Education, Science and Culture (J.K. and J.T.).

REFERENCES

BALLANYI K, ONIMARU H, HOMMA I (1999) Respiratory network function in the isolated brainstem-spinal cord of newborn rats. Prog Neurobiol 59: 583-634

BLAIR PS, FLEMING PJ, BENSLEY D, SMITH I, BACON C, TAYLOR E, BERRY J, GOLDING J, TRIPP J (1996) Smoking and the sudden infant death syndrome: Results from the 1993-5 case-control study for confidential inquiry into stillbirths and deaths in infancy. Brit Med J 313: 195-198

BURTON MD, NOURI M, KAZEMI H (1995) Acetylcholine and central respiratory control: Perturbations of acetylcholine synthesis in the isolated brainstem of the neonatal rat. Brain Res 670: 39-47

BURTON MD, JOHNSON D, KAZEMI H (1997) The central respiratory effects of acetylcholine vary with CSF pH. J Autonom Nerv Syst 62: 27-32

CHIODINI F, CHARPANTIER E, MULLER D, TASSONUI E, FUCHS-BUDER T, BERTRAND D (2001) Blockade and activation of the human neuronal nicotinic acetylcholine receptors by atracurium and laudanosine. Anesthesiology 94: 643-651

DOMINGUEZ DEL TORO E, JUIZ JM, PENG X, LINDSTROM J, CRIADO M (1994) Immunocytochemical localization of the alpha 7 subunit of the nicotinic acetylcholine receptor in the rat central nervous system. J Comp Neurol 349: 325-342

EUGENIN J, NICHOLLS JG (1997) Chemosensory and cholinergic stimulation of fictive respiration in isolated CNS of neonatal opossum. J Physiol, London 501: 425-437

EUGENIN J, LLONA I, INFANTE CD, AMPUERO E (2001) In vitro approach to the chemical drive of breathing. Biol Res 34: 117-122

FUCILE S, SUCAPANE A, EUSEBI F (2005) Ca2+ permeability of nicotinic acetylcholine receptors from rat dorsal root ganglion neurones. J Physiol 15(565,Pt 1): 219-28

GRAY R, RAJAN AS, RADCLIFFE KA, YAKEHIRO M, DANI JA (1996) Hippocampal synaptic transmission enhanced by low concentrations of nicotine. Nature 383: 713-716

HUANG YH, BROWN AR, COSTY-BENNETT S, LUO A, FREGOSI RF (2004) Influence of prenatal nicotine exposure on postnatal development of breathing pattern. Resp Physiol Neurobiol 143: 1-8

KUWANA S, OKADA Y, NATSUI T (1998) Effects of extracellular calcium and magnesium on central respiratory control in the brainstem-spinal cord of neonatal rat. Brain Res 786: 194-204

KUWANA S, OKADA Y, IWANAMI M (2000) Effects of

nicotinic ACh receptor antagonists on central respiratory chemosensitivity in the neonatal rat. Neurosci Res 24 (Suppl): S172

MCGEHEE DS, HEATH MJ, GELBER S, DEVAY P, ROLE LW (1995) Nicotine enhancement of fast excitatory synaptic transmission in CNS by presynaptic receptors. Science 269: 1692-1696

MELLEN NM, JANCZEWSKI WA, BOCCHIARO CM, FELDMAN JL (2003) Opioid-induced quantal slowing reveals dual networks for respiratory rhythm generation. Neuron 37: 821-826

MONTEAU R, MORIN D, HILAIRE G (1990) Acetylcholine and central chemosensitivity: *In vitro* study in the newborn rat. Respir Physiol 81: 241-254

MURAKOSHI T, SUZUE T, TAMAI S (1985) A pharmacological study on respiratory rhythm in the isolated brainstem-spinal cord preparation of the newborn rat. Bri J Pharmacol 86: 95-104

OKADA Y, CHEN Z, KUWANA S (2001) Cytoarchitecture of central chemoreceptors in the mammalian ventral medulla. Respir Physiol 129: 13-23

ONIMARU H, HOMMA I (1987) Respiratory rhythm generator neurons in medulla of brainstem-spinal cord preparation from newborn rat. Brain Res 403: 380-384

ONIMARU H, ARATA A, HOMMA I (1988) Primary respiratory rhythm generator in the medulla of brainstem-spinal cord preparation from newborn rat. Brain Res 445: 314-324

ONIMARU H, ARATA A, HOMMA I (1989) Firing properties of respiratory rhythm generating neurons in the absence of synaptic transmission in rat medulla in vitro. Exp Brain Res 76: 530-536

ONIMARU H, HOMMA I, IWATUKI K (1992) Excitation of inspiratory neurons by preinspiratory neurons in rat medulla in vitro. Brain Res Bull 29: 879-82

ONIMARU H, BALLANYI K, RICHTER DW (1996) Calcium-dependent responses in neurons of the isolated respiratory network of newborn rats. J Physiol 491: 677-695

ONIMARU H, ARATA A, HOMMA I (1997) Neuronal mechanisms of respiratory rhythm generation: an approach using in vitro preparation. Jpn J Physiol 47: 385-403

ONIMARU H, HOMMA I, (2003) A novel functional neuron group for respiratory rhythm generation in the ventral medulla. J Neurosci 23: 1478-1486

RICHERSON GB (1998) Cellular mechanisms of sensitivity to pH in the mammalian respiratory system. In: KAILA K, RANSOM BR (eds) pH and Brain Function. New York: Wiley-Liss. pp: 503-593

ROBINSON DM, PEEBLES KC, KWOK H, ADAMS BM, CLARKE LL, WOOLLARD GA, FUNK GD (2002) Prenatal nicotine exposure increases apnoea and reduces nicotinic potentiation of hypoglossal inspiratory output in mice. J Physiol 538: 957-973

SAKURABA S, KUWANA S, OCHIAI R, OKADA Y, KASHIWAGI M, HATORI E, TAKEDA J (2003) Effects of neuromuscular blocking agents on central respiratory control in the isolated brainstem-spinal cord of neonatal rat. Neurosci Res 47: 289-298

SAKURABA S, KUWANA S, ERIKSSON LI, OKADA Y, OCHIAI R, KASHIWAGI

M, HATORI E, LINDAHL SGE, TAKEDA J (2005) Effects of neuromuscular blocking agents on central respiratory chemosensitivity in newborn rats. Biol Res 38: 225-33

SHAO XM, FELDMAN JL (2000) Acetylcholine modulates respiratory pattern: effects mediated by M3-like receptors in preBötzinger complex inspiratory neurons. J Neurophysiol 83: 1243-1252

SHAO XM, FELDMAN JL (2001) Mechanisms underlying regulation of respiratory pattern by nicotine in preBötzinger complex. J Neurophysiol 85: 2461-2467

SHAO XM, FELDMAN JL (2002) Pharmacology of nicotinic receptors in preBötzinger complex that mediate modulation of respiratory pattern. J Neurophysiol 88: 1851-1858

SHAO XM, FELDMAN JL (2005) Cholinergic neurotransmission in the preBötzinger Complex modulates excitability of inspiratory neurons and regulates respiratory rhythm. Neuroscience 130: 1069-1081

SMITH JC, ELLENBERGER HH, BALLANYI K, RICHTER DW, FELDMAN JL (1991) Pre-Bötzinger complex: A brain stem region that may generate respiratory rhythm in mammal. Science 254: 716-719

TAKEDA S, ERIKSSON LI, YAMAMOTO Y, JOENSEN H, ONIMARU H, LINDAHL SG (2001) Opioid action on respiratory neuron activity of the isolated respiratory network in newborn rats. Anesthesiology 95: 740-749

WADA E, WADA K, BOULTER J, DENERIS E, HEINEMANN S, PATRICK J, SWANSON LW (1989) Distribution of alpha 2, alpha 3, alpha 4, and beta 2 neuronal nicotinic receptor subunit mRNAs in the central nervous system: a hybridization histochemical study in the rat. J Comp Neurol 284: 14-335

WONNACOTT S (1997) Presynaptic nicotinic ACh receptors. Trends Neurosci 20: 92-98

Contribution of High-Mobility Group Box-1 to the Development of Ventilator-induced Lung Injury

Eileen N. Ogawa, Akitoshi Ishizaka, Sadatomo Tasaka, Hidefumi Koh, Hiroshi Ueno, Fumimasa Amaya, Masahito Ebina, Shingo Yamada, Yosuke Funakoshi, Junko Soejima, Kiyoshi Moriyama, Toru Kotani, Satoru Hashimoto, Hiroshi Morisaki, Edward Abraham, and Junzo Takeda

Departments of Anesthesiology and Medicine, School of Medicine, Keio University; Department of Anesthesiology and Intensive Care, Tokyo Women's Medical University Daini Hospital, Tokyo; Department of Anesthesiology and Intensive Care, Kyoto Prefectural University of Medicine, Kyoto; Respiratory Oncology and Molecular Medicine, Institute of Development, Aging, and Cancer, Tohoku University, Sendai; Central Institute, Shino-Test Corporation, Kanagawa; Ono Pharmaceutical Co. Ltd., Osaka, Japan; and Department of Medicine, University of Alabama, Birmingham, Alabama

Rationale: Proinflammatory cytokines play an important role in ventilator-induced lung injury (VILI). High-mobility group box-1 (HMGB1) is a macrophage-derived proinflammatory cytokine that can cause lung injury.

Objectives: This study tested the hypothesis that HMGB1 is released in intact lungs ventilated with large V_T. A second objective was to identify the source of HMGB1. A third objective was to examine the effects of blocking HMGB1 on the subsequent development of VILI.

Methods: Bronchoalveolar lavage fluid (BALF) and lung tissues were obtained from rabbits mechanically ventilated for 4 h with a small (8 ml/kg) versus a large (30 ml/kg) V_T. BALF was also obtained from rabbits with intratracheal instillation of anti-HMGB1 antibody before the initiation of large V_T ventilation.

Measurements and Main Results: The concentrations of HMGB1 in BALF were fivefold higher in the large than in the small V_T group. Immunohistochemistry and immunofluorescence studies revealed expression of HMGB1 in the cytoplasm of macrophages and neutrophils in lungs ventilated with large V_T. Blocking HMGB1 improved oxygenation, limited microvascular permeability and neutrophil influx into the alveolar lumen, and decreased concentrations of tumor necrosis factor-α in BALF.

Conclusions: These observations suggest that HMGB1 could be one of the deteriorating factors in the development of VILI.

Keywords: high-mobility group box-1; macrophage, rabbit model; ventilator-induced lung injury

Although mechanical ventilation is an essential support in patients suffering from severe respiratory failure (e.g., acute respiratory distress syndrome [ARDS]), clinical and experimental observations have shown that it can be harmful under some conditions (1, 2). Because the pathologic changes of ARDS are inhomogeneously distributed in the lungs, less diseased areas can be overstretched by mechanical ventilation, causing ventilator-induced lung injury (VILI) (3–5). Besides mechanical stretch and shear stress, inflammatory cytokines produced in the lung, including tumor necrosis factor (TNF)-α, interleukin (IL)-1β, IL-6, IL-10, macrophage inflammatory protein (MIP)-2 (a rodent homolog of IL-8), IFN-γ (6), and IL-8 (7) promote VILI (8).

High-mobility group box-1 (HMGB1), a nonhistone, chromatin-associated protein produced by nearly all cell types (9), has been identified as a late mediator of endotoxin lethality and acute lung inflammation in mice (10). Elevated serum concentrations of HMGB1 in septic patients are a marker of poor prognosis (10), and HMGB1 levels are increased in the plasma and lung epithelial lining fluid of patients with acute lung injury (ALI) (11). ALI, with accumulation of neutrophils, development of interstitial edema, and increased production of IL-1β, IL-1Ra, TNF-α, and MIP-2 in the lungs, occurs within 24 h after the intratracheal administration of HMGB1 in mice (11, 12). HMGB1 is secreted by macrophages 8 h after stimulation with endotoxin and 18 h after stimulation with IL-1β and TNF-α (10). Necrotic or injured cells can also passively release HMGB1 (13).

Although HMGB1 has potent inflammatory properties that contribute to the development of ALI, its involvement in VILI has not been examined. Therefore, this study tested the hypothesis that HMGB1 is released in intact lungs ventilated with large V_T. A second objective was to identify the source of HMGB1 by immunohistochemical staining of lung tissue and immunofluorescence studies of inflammatory cells in overinflated lungs. A third objective was to examine the effects of blocking HMGB1 on the subsequent development of VILI.

METHODS

An expanded methods description can be found in the online supplement. Our experimental protocol was approved by the Council on Animal Care of Keio University and was in compliance with the guidelines of the National Institutes of Health. We studied 47 male Japanese White rabbits. The nonventilated group included six rabbits without mechanical ventilation. After tracheotomy, 12 rabbits were randomly assigned to a group ventilated with a V_T of 8 ml/kg (small V_T group, n = 6) versus 30 ml/kg (large V_T group, n = 6). Bronchoalveolar lavage fluid (BALF) from the right lung and blood was collected after 4 h of ventilation. The left lung was used to measure the wet-to-dry weight (W/D) ratio. All rabbits received 5 mg of human serum albumin (HSA) intravenously 1 h before death to determine the lung permeability index, which is defined as the HSA in BALF-to-plasma ratio expressed as a percentage (14). The concentrations of HSA, IL-8, TNF-α, and HMGB1 (15) were measured by ELISA. The activity of lactate dehydrogenase (LDH) was analyzed by spectrophotometric assay. The BALF sediments were used for white blood cell (WBC) and differential cell counts.

To locate HMGB1, immunohistochemical studies were performed using specimens from nine rabbits randomly assigned to one of a nonventilated group, a small V_T group, or a large V_T group (n = 3 in each group). The specimens were counterstained with hematoxylin–eosin and elastica-Masson stains. A blind coexperimenter counted the numbers of macrophages and neutrophils per millimeters squared in 10 randomly

(Received in original form September 1, 2005; accepted in final form May 25, 2006)

Supported by the Keio Gijuku Postgraduate School Fund for the Advancement of Research and by a grant-in-aid for Fundamental Scientific Research from the Education Ministry of Japan 07670678 (A.I.) and 16390457 (S.H.).

Correspondence and requests for reprints should be addressed to Akitoshi Ishizaka, M.D., Ph.D., Department of Medicine, School of Medicine, Keio University, 35 Shinanomachi, Shinjuku-ku, Tokyo 160-8582, Japan. E-mail: ishizaka@cpnet.med.keio.ac.jp

This article has an online supplement, which is accessible from this issue's table of contents at www.atsjournals.org

Am J Respir Crit Care Med Vol 174. pp 400–407, 2006
Originally Published in Press as DOI: 10.1164/rccm.200605-699OC on May 25, 2006
Internet address: www.atsjournals.org

chosen views. Immunofluorescence staining for HMGB1 was also performed in macrophages and neutrophils collected from BALF. The inflammatory cells from a lung ventilated for 4 h with a 30 ml/kg VT were assigned to the large VT group, and the cells from a nonventilated lung were divided into a control and a LPS-stimulated group. In the latter group, 1 pg/ml of LPS was added, and cells were incubated for 4 h. HMGB1 was visualized by an indirect immunofluorescence technique.

In the HMGB1-blockade study, 18 rabbits were randomly and evenly assigned to a normal saline group, a control antibody group, or an anti-HMGB1 antibody group, which, respectively, received intratracheally 1 ml of sterile saline, 2 mg of nonspecific isotype-specific antibody, or 2 mg of anti-HMGB1 antibody (Shino-test, Kanagawa, Japan) dissolved in 1 ml of sterile saline (14). After 4 h of ventilation with a 30-ml/kg VT, BALF from the right upper lung and the blood was collected. The right lower lobe was used to measure the W/D ratio.

The data were analyzed by the StatView version 5.0 software (Abacus Concepts, Berkeley, CA). Because the data for cell count in immunohistochemistry could not assume the normal distribution, nonparametric analysis was used. Other data were analyzed by one-way analysis of variance followed by Fisher's test for the comparison among three groups and unpaired Student's *t* test for the comparison between two groups. Statistical significance was set at $p < 0.05$. The results are expressed as means ± SEM.

RESULTS

Effects of Mechanical Ventilation on the Release of HMGB1 in the Lung

The ventilatory settings and the blood gas analyses in each group are summarized in the online supplement (Tables E1 and E2 in the online supplement). The respiratory rate was higher in the small VT group to maintain a stable Pa_{CO_2} partial pressure. In the large VT group, P_{O_2} was lower and P_{CO_2} was higher after 4 h than after 2 h of ventilation, although the differences in arterial blood gases between the two VT groups at the same time points did not reach statistical significance. There were no significant differences in hemodynamic measurements between the small and the large VT groups (data not shown).

Permeability index and W/D ratio. The permeability index was higher in the large than in the small VT group after 4 h of mechanical ventilation (Figure 1A). Likewise, the W/D ratio was greater in the large VT group than in the nonventilated and the small VT groups (Figure 1B).

LDH in BALF and plasma. The LDH activity in BALF was significantly higher in the large VT group than in the control or the small VT group (Figure 1C). Plasma LDH activity was higher in the small VT (158 ± 23 IU/L, $p < 0.01$, vs. the nonventilated group) and the large VT (139 ± 9 IU/L, $p < 0.05$, vs. the nonventilated group) groups than in the nonventilated group (56.9 ± 14.1 IU/L).

WBC counts. Marked neutrophil accumulation in BALF was observed in the large VT group, whereas the macrophage counts were similar among the study groups (Figure 1D). The number of neutrophils did not differ from that of macrophages in the large VT group.

HMGB1 in BALF and plasma. The concentrations of HMGB1 in BALF and plasma are shown in Figure 2A. The HMGB1 concentration in BALF of the large VT group was significantly higher than in the other groups. HMGB1 was undetectable or nearly undetectable in most plasma samples.

IL-8 and TNF-α in BALF and plasma. The concentration of IL-8 in BALF was significantly higher in the large VT group than in the nonventilated or the small VT groups (Figure 2B). Similarly, the concentration of IL-8 in plasma was higher in the large VT group than in the two other groups (nonventilated group, 93.4 ± 30.6 pg/ml; small VT group, 79.8 ± 21.1 pg/ml; large VT group, 175 ± 25 pg/ml; $p < 0.05$). The TNF-α concentration in

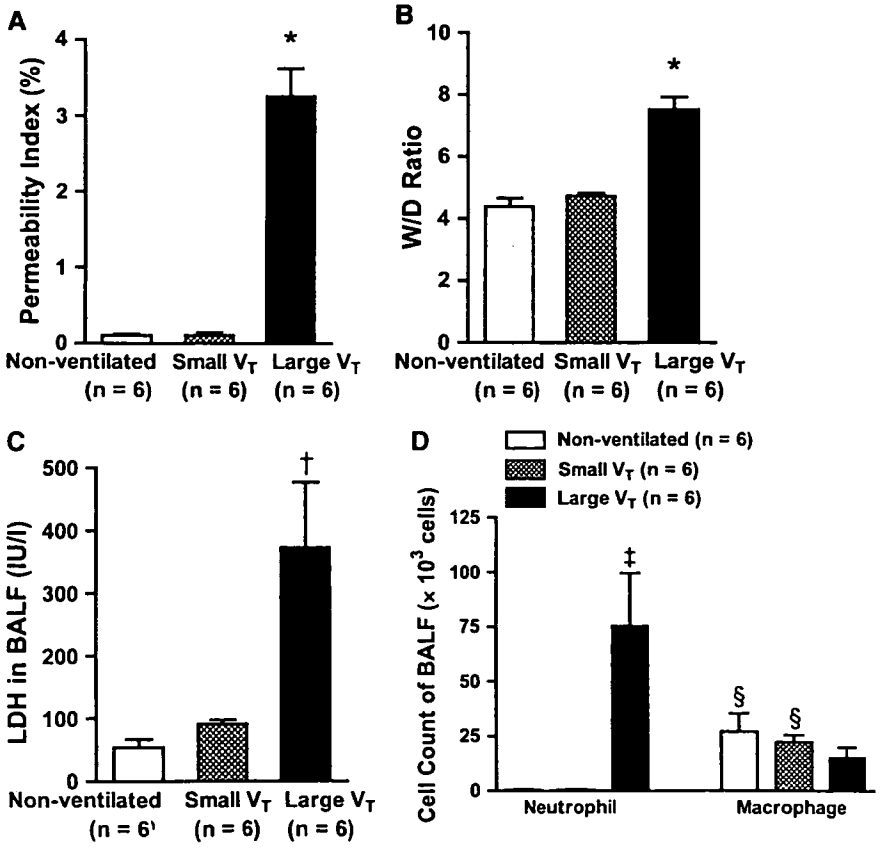

Figure 1. Effect of mechanical ventilation on lung permeability, wet-to-dry (W/D) weight ratio, lactate dehydrogenase (LDH) release, and the accumulation of inflammatory cells in lungs with no mechanical ventilation versus lungs ventilated with a small (8 ml/kg) or a large VT (30 ml/kg) for 4 h. (*A*) Lung albumin permeability index. (*B*) W/D ratio in left lobes. (*C*) LDH in bronchoalveolar lavage fluid (BALF). (*D*) Neutrophil and macrophage counts in BALF. Values are means ± SEM. n = 6 in each group. *$p < 0.0001$ versus the nonventilated and small VT groups. †$p < 0.05$ versus the nonventilated and small VT groups. ‡$p < 0.01$ versus the nonventilated and small VT groups. §$p < 0.05$ versus neutrophils in the same group.

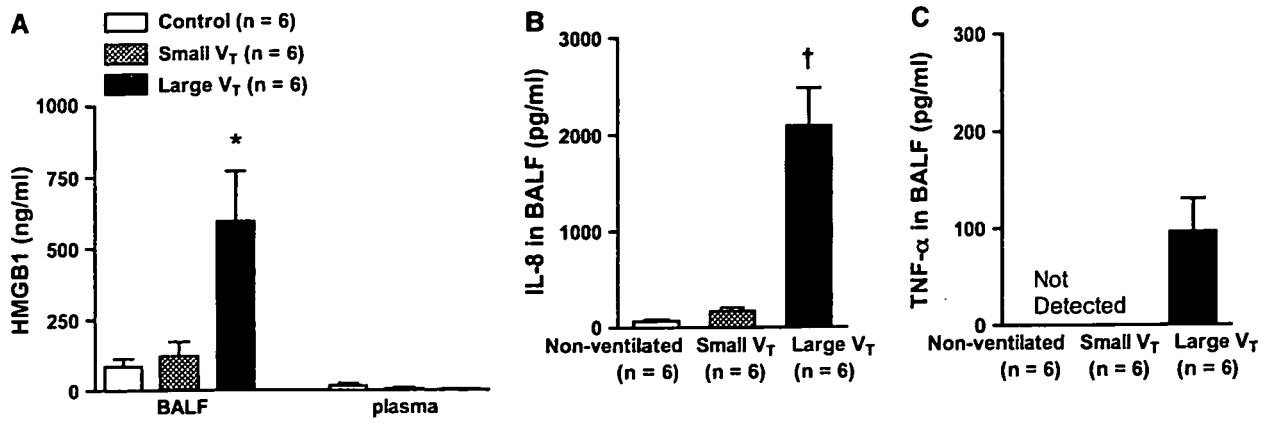

Figure 2. Concentration of high-mobility group box-1 (HMGB1) in plasma and concentrations of HMGB1, interleukin (IL)-8, and tumor necrosis factor (TNF)-α in bronchoalveolar lavage fluid (BALF) of lungs with no mechanical ventilation and in BALF of lungs ventilated with a small (8 ml/kg) or a large VT (30 ml/kg) for 4 h. (*A*) HMGB1 concentration in BALF and plasma. (*B*) IL-8 concentration in BALF. (*C*) TNF-α concentration in BALF. TNF-α was detected in the large VT group only. Values are means ± SEM. n = 6 in each group. *$p < 0.05$ versus the nonventilated and small VT groups. †$p < 0.0001$ versus the nonventilated and small VT groups.

BALF was 96.5 ± 33.8 pg/ml in the large VT group and was undetectable in the other two groups (Figure 2C). The concentrations of TNF-α in plasma did not show significant differences (nonventilated group, 135 ± 62 pg/ml; small VT group, 254 ± 129 pg/ml; large VT group, 18.7 ± 17.5 pg/ml).

HMGB1 Immunohistochemistry

The lungs with no mechanical ventilation (Figure 3A) and with the small VT ventilation (Figure 3B) contained sparsely distributed inflammatory cells that were mostly not immunoreactive for HMGB1. Alveolar hemorrhage and interstitial congestion and thickening were limited to lungs exposed to the large VT ventilation, which also demonstrated increased numbers of alveolar macrophages and infiltration of many neutrophils (Figure 3C). Some macrophages and neutrophils that had migrated into the alveolar spaces during the large VT ventilation were intensely immunoreactive for HMGB1 (Figure 3D). Only a subset of alveolar epithelial cells was also immunoreactive for HMGB1. The injured lung tissues had no immunohistochemical staining with irrelevant antibody (Figure 3E).

WBC counts. The numbers of HMGB1-negative neutrophils or macrophages did not show significant differences among the groups, but the numbers of HMGB1-positive neutrophils and macrophages increased significantly in the large VT group compared with the nonventilated group (Figures 4A and 4B). There were no significant differences between the total cell counts for neutrophils and macrophages in each group.

Immunofluorescence of Inflammatory Cells for HMGB1

To identify the source of HMGB1 released in the lung during large VT ventilation, we performed immunohistochemistry using anti-HMGB1 antibodies. Unstimulated alveolar macrophages collected from the lung with no mechanical ventilation (control group) did not stain for HMGB1 (Figure 5A), whereas those stimulated with LPS (LPS-stimulated group) stained prominently for HMGB1 (Figure 5B). Similarly, macrophages collected from the lung ventilated with a large VT were positively stained for HMGB1 (Figure 5C), whereas there was no expression of HMGB1 on neutrophils from control lungs and lungs ventilated with a large VT.

Effect of Intratracheal Instillation of Anti-HMGB1 Antibody on VILI

There were no significant differences in ventilatory settings (data not shown), pH, and Pco_2 among the study groups treated with normal saline, anti-HMGB1, or control antibodies (Table E3). After 4 h of ventilation, Po_2 was significantly higher in the anti-HMGB1 antibody group compared with both other groups (normal saline group: 57.4 ± 4.1 mm Hg, $p < 0.01$, vs. the anti-HMGB1 antibody group; control antibody group: 59.8 ± 9.0 mm Hg, $p = 0.01$, vs. the anti-HMGB1 antibody group; anti-HMGB1 antibody group: 106 ± 18 mm Hg).

Permeability index and W/D ratio. The permeability index was significantly lower in the anti-HMGB1 antibody group than in the normal saline group or in the control antibody group (Figure 6A), whereas the W/D ratio was similar among the study groups (Figure 6B).

LDH in BALF and plasma. The LDH activity in BALF was significantly lower in the control antibody group than in the normal saline group and was lowest in the anti-HMGB1 antibody group (Figure 6C). Plasma LDH activity was significantly lower in the anti-HMGB1 antibody group (81.1 ± 6.7 IU/L) than in the normal saline group (234 ± 56 IU/L; $p < 0.01$ vs. the anti-HMGB1 antibody group), whereas LDH in the control antibody group (140 ± 7.8 IU/L) was intermediate.

WBC counts. The number of neutrophils in the BALF was lower in the control antibody and the anti-HMGB1 antibody groups than in the normal saline group. Macrophage counts were similar among the groups (Figure 6D).

IL-8 and TNF-α in BALF and plasma. The concentration of IL-8 in the BALF was similar among the study groups (Figure 7A). There was a significant difference in the plasma concentration of IL-8 between the control antibody group (257 ± 19 pg/ml) and the anti-HMGB1 antibody group (181 ± 16 pg/ml; $p < 0.05$ vs. the control antibody group), whereas the levels of IL-8 in the normal saline group (211 ± 31 pg/ml) were intermediate between the two other groups. BALF TNF-α was significantly higher in the normal saline and control antibody groups than in the anti-HMGB1 antibody group (Figure 7B). The concentrations of TNF-α in plasma were similar among the three groups (normal saline group, 480 ± 119 pg/ml; control antibody group, 506 ± 143 pg/ml; anti-HMGB1 antibody group, 260 ± 131 pg/ml)

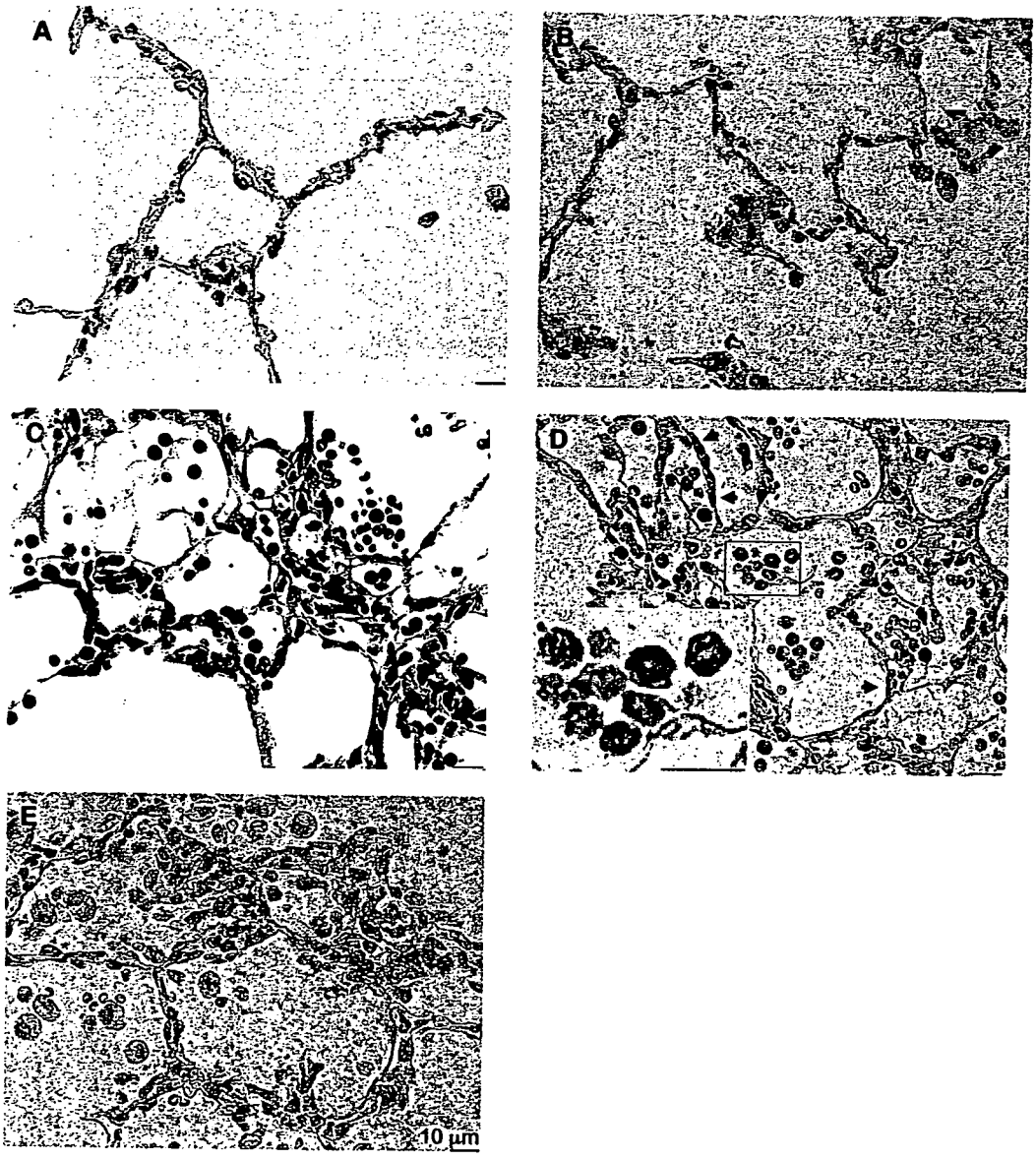

Figure 3. Immunohistochemical staining of lung sections for HMGB1. (*A*) In lungs with no mechanical ventilation, there was no immunoreaction. (*B*) The lungs ventilated with a small V_T (8 ml/kg) for 4 h had a fraction of immunoreactive inflammatory cells. (*C*) In lungs ventilated with a large V_T (30 ml/kg) for 4 h, numerous neutrophils have infiltrated in the alveolar walls and alveolar space (hematoxylin and eosin stain). (*D*) Macrophages and neutrophils infiltrated in the lungs injured by large V_T were immunoreactive for HMGB1 (*stained in brown*). A subset of alveolar epithelial cells was also immunoreactive (*arrows*). The *inset* shows enlargement of an enclosed area. (*E*) The injured lung tissues had no immunohistochemical staining with irrelevant antibody. Original magnification: ×1,000.

DISCUSSION

Our study provides three observations. First, ventilation with a large V_T caused prominent VILI in our rabbit model, which was associated with fivefold higher HMGB1 concentrations in BALF than ventilation with a small V_T. Second, immunostaining showed that the sources of HMGB1 were not only alveolar macrophages but also neutrophils. Third, measurements of microvascular permeability and oxygenation revealed that lung injury caused by ventilation with a large V_T could be mitigated by pretreatment with anti-HMGB1 antibody. Furthermore, administration of anti-HMGB1 antibody significantly reduced the VILI-induced elevations of TNF-α in the BALF while leaving IL-8 concentrations unchanged.

In preliminary studies in rabbits, we observed that the degree of ALI caused by 4 h of mechanical ventilation was dependent on V_T. Although a V_T of 30 ml/kg caused prominent lung injury, 20 ml/kg was not associated with an increase in W/D ratio. We had previously shown that mechanical ventilation with a V_T of 20 ml/kg caused an infiltration of neutrophils, increased the IL-8 concentration in BALF (16), and enhanced the expression of CD14 protein on alveolar macrophages (17). It has also been reported that rabbit lungs mechanically ventilated for 6 h with a V_T of 10 ml/kg develop an increase in W/D ratio and upregulated gene expression of monocyte chemoattractant protein-1, TNF-α, and IL-1β, although there was no increase in the protein concentrations of these cytokines (18). In a rat model of acid-induced lung injury, lungs mechanically ventilated for 4 h with a 12 ml/kg V_T and 10 cm H_2O positive end-expiratory pressure, with a plateau pressure of approximately 30 cm H_2O, a pressure similar to that used in the large V_T group in the present study, developed alveolar epithelial and endothelial injury compared with lungs ventilated with a smaller V_T (19). In an *ex vivo* model of VILI, rat lungs mechanically ventilated with a V_T of 15 ml/kg for 2 h developed increased concentrations of TNF-α, IL-1β, IL-6, IL-10, MIP-2, and IFN-γ in BALF, which increased further when V_T was increased to 40 ml/kg (6). ALI and ARDS are not pathologically homogeneous in the lung, with some areas being less affected and more compliant (4, 5). Regions of the lung may be mechanically overstretched even by normal V_T ventilation. We chose the V_T of 30 ml/kg in this study because it caused evident VILI with significant increase in permeability index and W/D ratio.

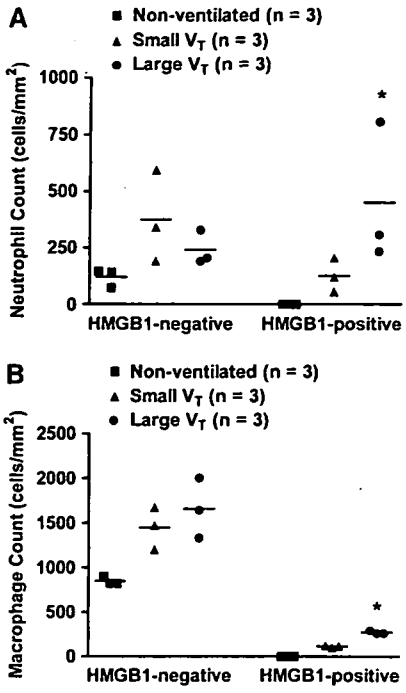

Figure 4. Effect of mechanical ventilation on the accumulation of inflammatory cells in lungs with no mechanical ventilation versus lungs ventilated with a small (8 ml/kg) or a large VT (30 ml/kg) for 4 h in immunohistochemical staining for HMGB1. (*A*) Neutrophil counts per mm² in 10 randomly chosen views in the lung section. (*B*) Macrophage counts per mm² in 10 randomly chosen views in the lung section. A *horizontal bar* represents a mean value in each group. n = 3 in each group. *p < 0.05 versus the nonventilated group.

Ueno and colleagues reported that HMGB1 was increased in the lung epithelial lining fluid of patients with ALI (11), and previous animal studies demonstrated increased pulmonary HMGB1 concentrations in models of endotoxin- or hemorrhage-induced lung injury (11, 20). Because our intent was to identify the role played by HMGB1 in the development of VILI, we limited the stimulation to mechanical stress produced by the large VT ventilation in intact rabbit lungs.

LDH in BALF was fourfold higher in the group ventilated with a large VT than in that exposed to a small VT. When alveolar type II cells are exposed to mechanical stretch at an increased amplitude or frequency, the release of LDH from the cells is increased in association with their apoptosis and necrosis (21). Because HMGB1 is present in most cell types (9) and can be passively released from necrotic cells (12, 22), it may be released into BALF from injured epithelial cells in VILI. The results of the immunohistochemical study, showing HMGB1-immunoreactive epithelial cells, support this view, although further studies are needed to measure the release of HMGB1 from each cell type.

There was a discrepancy in the inflammatory cell count between the BALF and immunohistochemistry in the large VT group. Although there were no significant differences between macrophage and neutrophil counts in BALF and by immunohistochemistry, macrophages tended to be fewer than neutrophils in the BALF, whereas macrophages tended to be greater in the lung specimen. It is reported that after 40 min of high-pressure (peak inspiratory pressure [PIP] of 45 cm H_2O) ventilation, macrophages decreased in the BALF of rat lungs, whereas neutrophils increased (23). There was also greater expression of intercellular adhesion molecule-1 (ICAM-1) and macrophage antigen-1 on alveolar macrophages in the high-pressure group. Our results support the view that alveolar macrophages tend to stay in the alveolar spaces during BAL, resulting in artificially low numbers of cells in the BALF.

In the lung ventilated with a 30 ml/kg VT, some alveolar macrophages and neutrophils were intensely immunoreactive for HMGB1. The immunofluorescence experiments confirmed the positive expression of HMGB1 in the cytoplasm of macrophages collected from the lung ventilated with a large VT. It has

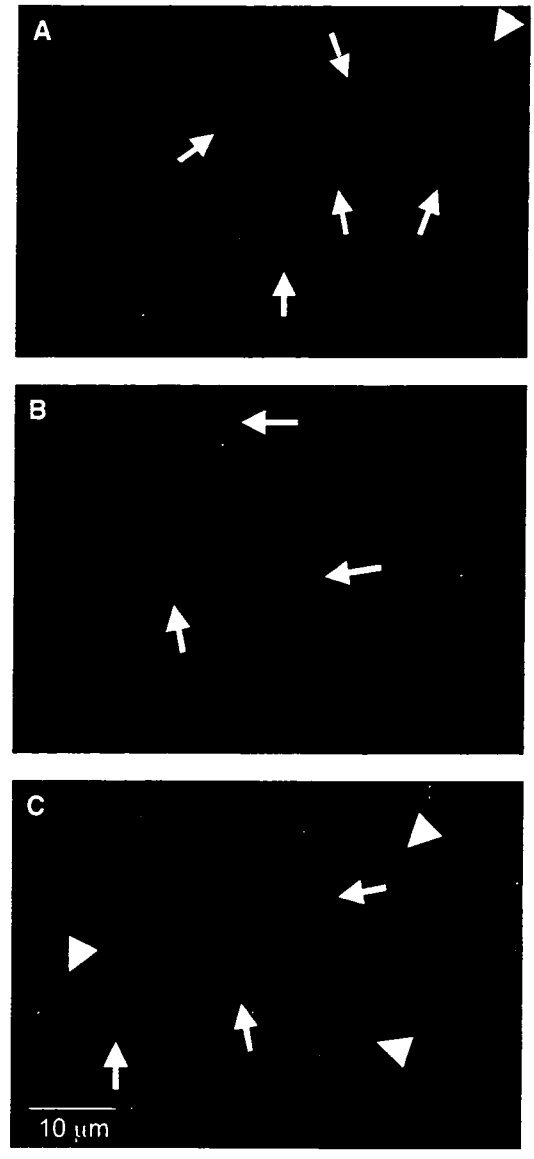

Figure 5. Immunofluorescence staining of macrophages for HMGB1. The *red* Cy3 signal shows immunostaining against HMGB1, and the *blue* signal shows nuclear staining with 4,6-diamidino-2-phenylindole. (*A*) Macrophages collected from a lung with no mechanical ventilation (*arrows*). (*B*) Macrophages collected from a lung with no mechanical ventilation and incubated for 4 h with LPS (*arrows*). (C) Macrophages collected from a lung ventilated with a large VT (30 ml/kg) for 4 h (*arrows*). No staining was observed in unstimulated macrophages (*A*). Macrophages incubated with LPS (*B*) or collected from an overventilated lung (C) were stained, whereas the neutrophils collected from normal or overventilated lungs were not stained for HMGB1 (*arrowheads*). Original magnification: ×400.

been reported that, in the resting state, macrophages contain HMGB1 in their nucleus while a fraction of HMGB1 is transferred to cytoplasmic vesicles after stimulation with LPS (24). After intratracheal instillation of LPS in mice, nuclear and cytoplasmic expression of HMGB1 was observed in the alveolar macrophages (11). Our study further shows that mechanical ventilation with a large VT stimulates macrophages and neutrophils and increases their cytoplasmic content of HMGB1, although it is unknown whether the HMGB1 in the cytoplasm comes out from the nucleus into the cytoplasm or is produced in the cytoplasm of macrophages and neutrophils. The aspect of mechanical

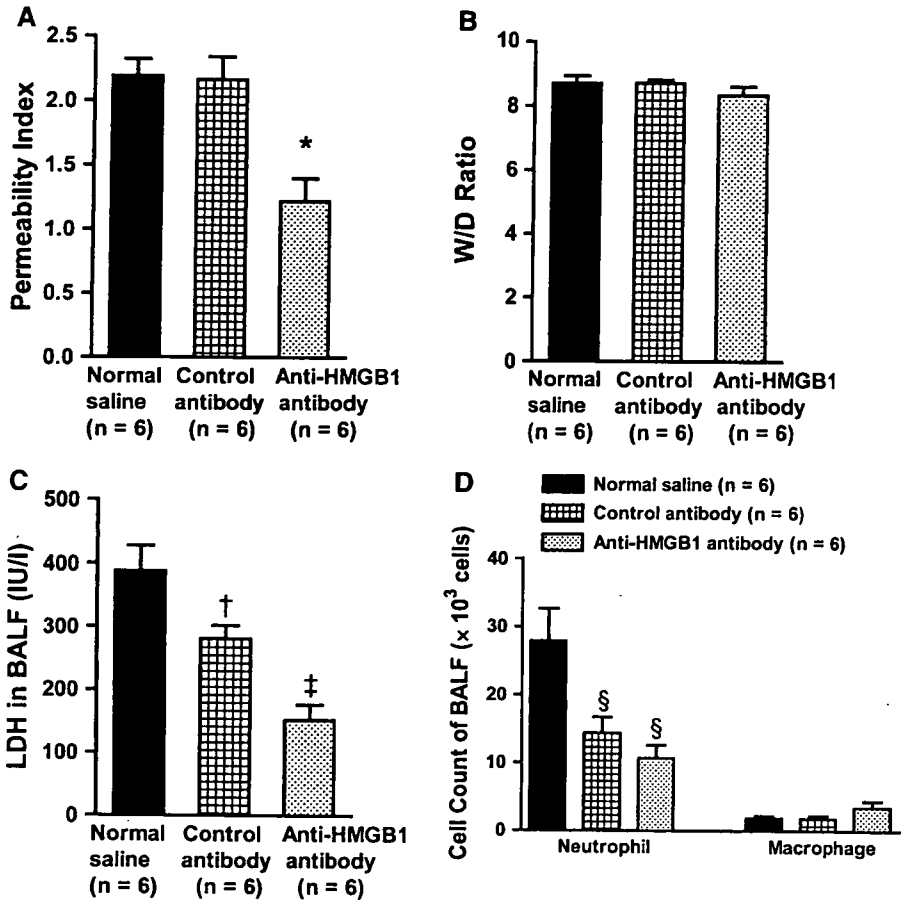

Figure 6. Effect of intratracheal instillation of normal saline, control antibody, or anti-HMGB1 antibody on lung permeability, W/D weight ratio, LDH release, and the accumulation of inflammatory cells in the lungs after mechanical ventilation with a large VT (30 ml/kg) for 4 h. (*A*) Lung albumin permeability index. (*B*) W/D ratio in right lower lobes. (*C*) LDH in BALF. (*D*) Neutrophil and macrophage counts in BALF. Values are means ± SEM. $n = 6$ in each group. *$p < 0.001$ versus the normal saline and control antibody groups. †$p < 0.05$ versus the normal saline group. ‡$p < 0.0001$ versus the normal saline group, and $p < 0.01$ versus the control antibody group. §$p < 0.01$ versus the normal saline group.

ventilation, whether stretch, shear stress, or increased cytokine concentrations, that is most important for inducing the production of HMGB1 by macrophages and neutrophils also remains to be determined. Although TNF-α is one of the potential mediators that could cause the release of HMGB1 from macrophages, 4 h of mechanical ventilation seems too short for this mechanism to be operative because in the study by Wang and colleagues, no increase in HMGB1 was observed earlier than 18 h after stimulating murine macrophage-like cells with TNF-α *in vitro* (10).

Neutrophils are an alternate source of HMGB1. Although our immunofluorescence experiments did not show HMGB1 expression in neutrophils collected from the lung ventilated with a large VT, neutrophils were immunoreactive for HMGB1 in the immunohistochemical study. At sites of acute inflammation, some neutrophils undergo necrosis, whereas others undergo apoptosis (25). During apoptosis, the surface of neutrophils remains intact, and they can be cleared by macrophages without leaking their potentially injurious contents. However, if macrophages fail to rapidly clear apoptotic neutrophils, the latter undergo secondary necrosis (25). Neutrophils that undergo necrosis cannot be stained by immunofluorescence, although the leakage of HMGB1 from necrotic cells could contribute to its increase in BALF. Because neutrophils in the large VT group were immunoreactive for HMGB1 in the immunohistochemical study, the secretion of HMGB1 from neutrophils has not been excluded as a possible explanation.

The reduction in severity of ALI caused by intratracheal instillation of anti-HMGB1 antibodies is consistent with previous reports showing that anti-HMGB1 reduces endotoxin lethality (10) and attenuates LPS-induced ALI (11, 12). Abraham and colleagues reported that treatment with anti-HMGB1 had no effect on TNF-α or MIP-2 protein concentrations in endotoxin-induced ALI (12). Although the measurements of IL-8 in our study, which showed no change in its concentrations after the instillation of anti-HMGB1 antibody, are concordant with that report, the measurements of TNF-α, which showed decreases in concentration after the treatment, were not.

IL-8 is a potent neutrophil chemoattractant that modulates the development of ALI (26, 27) and is produced by bronchial epithelial cells, alveolar epithelium, alveolar macrophages, and smooth muscles of pulmonary vessels after 4 h of mechanical ventilation with a VT of 20 ml/kg (16). In our study, the release of IL-8 into the BALF was increased by ventilation with a large VT, consistent with previous observations (16, 28, 29). HMGB1 activates the gene expression of IL-8 in neutrophils after a period of 30 min to 4 h (30) and stimulates the release of IL-8 from monocytes within 4 h (31). Although neutrophil infiltration was suppressed in anti-HMGB1–treated animals, IL-8 was not decreased after treatment with intratracheal anti-HMGB1 antibodies.

We observed decreased LDH concentration and neutrophil counts in BALF after intratracheal instillation of control antibody compared with normal saline. These findings suggest that instillation of polyclonal antibodies might have suppressive effect on the production of cytokines and other inflammatory mediators in VILI, although the detailed mechanism remains unclear.

In a murine model of endotoxin-induced ALI, treatment with anti-HMGB1 antibodies before or after the administration of endotoxin significantly suppressed the accumulation of neutrophils into the lungs but had no effect on the production of MIP-2

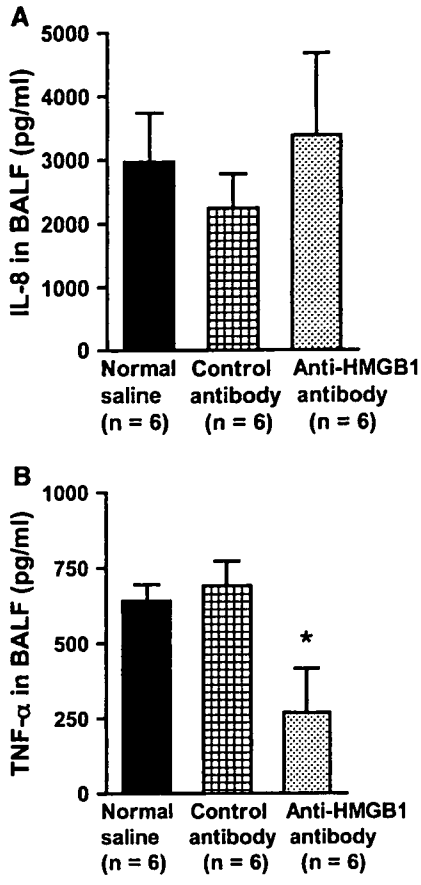

Figure 7. IL-8 and TNF-α concentrations in BALF after intratracheal administration of normal saline, control antibody, or anti-HMGB1 antibody followed by subsequent mechanical ventilation with a large VT (30 ml/kg) for 4 h. (*A*) IL-8 concentration in BALF. (*B*) TNF-α concentration in BALF. Values are means ± SEM. n = 6 in each group. *p < 0.05 versus the normal saline and control antibody groups.

(12). Because HMGB1 increases the expression of ICAM-1 and vascular cell adhesion molecule-1 (VCAM-1) on human endothelial cells (32, 33), blockade of HMGB1 may have decreased the expression of ICAM-1 and VCAM-1 on the lung endothelial cells and, consequently, may have limited the appearance of neutrophils in the BALF. Future studies are necessary to examine further interaction between HMGB1 and ICAM-1/VCAM-1 in the development of VILI.

There is discordance among studies regarding the release of TNF-α in VILI. In some studies, mechanical ventilation *per se* did not cause the release of detectible amounts of TNF-α (16, 28, 34), whereas it did in others (6). In the current study, release of TNF-α into the BALF was observed only in the large VT group. This observation may be explained by the stimulation of TNF-α synthesis in monocytes within 3 h by HMGB1 (31) and by its activation of the gene expression of TNF-α in neutrophils after a period of 30 min to 4 h (30). The decrease in TNF-α concentrations in BALF by treatment with anti-HMGB1 antibodies suggests that HMGB1 in the BALF plays an important role in the regulation of TNF-α production in VILI. TNF-α also enhances the expression of ICAM-1 and VCAM-1 on human endothelial cells (35, 36). The decreased number of neutrophils after blockade of HMGB1 might be due to lower concentrations of TNF-α, which decreased the expression of ICAM-1 and VCAM-1 on the lung endothelial cells.

The discrepancy between the permeability index and the W/D ratio in the HMGB1 blockade study could be the result of the difference in the sensitivity and the specificity of each measurement because the value of permeability index of the large VT group was 30 times that of the nonventilated group, whereas the W/D ratio showed only 1.7 times difference. The permeability index with HSA might be able to detect a slight change in the lung microvascular permeability. Because HSA was given intravenously 1 h before the animals were killed and calculated as the ratio of its concentration in BALF to plasma at the time point of death, the permeability index might only represent the leakage of the HSA from plasma during this 1 h, whereas the W/D ratio represents the amount of water in the lung accumulating through the whole experimental time.

Administration of HMGB1 in high doses causes death in mice within 18 to 36 h (10), and an acute, diffuse inflammatory response has been observed 24 h after its intratracheal instillation (11, 12). The present experiments showed that the intratracheal instillation of anti-HMGB1 antibody reduced the release of LDH and limited the increase in microvascular permeability after 4 h of injurious mechanical ventilation, preserving cell integrity and oxygenation. Although it is a late mediator of LPS, HMGB1 might express its toxicity in a short period of time in VILI.

In conclusion, mechanical ventilation with a large VT alone can increase HMGB1 in the alveolar space, partially contributing to the pathogenesis of VILI. Although the mechanism by which blockade of HMGB1 reduces the severity of VILI-induced ALI needs to be further studied, these results suggest that HMGB1 may be an appropriate therapeutic target in VILI.

Conflict of Interest Statement: None of the authors has a financial relationship with a commercial entity that has an interest in the subject of this manuscript.

Acknowledgment: The authors thank Michiko Yamamoto, B.S., for technical support and Ikuro Maruyama, M.D., for valuable advice.

References

1. The Acute Respiratory Distress Syndrome Network. Ventilation with lower tidal volumes as compared with traditional tidal volumes for acute lung injury and the acute respiratory distress syndrome. *N Engl J Med* 2000;342:1301–1308.
2. Dreyfuss D, Saumon G. Ventilator-induced lung injury: lessons from experimental studies. *Am J Respir Crit Care Med* 1998;157:294–323.
3. Gattinoni L, D'Andrea L, Pelosi P, Vitale G, Pesenti A, Fumagalli R. Regional effects and mechanism of positive end-expiratory prssure in early adult respiratory distress syndrome. *JAMA* 1993;269:2122–2127.
4. Gattinoni L, Presenti A, Torresin A, Baglioni S, Rivolta M, Rossi F, Scarani F, Marcolin R, Cappelletti G. Adult respiratory distress syndrome profiles by computed tomography. *J Thorac Imaging* 1986;1: 25–30.
5. Maunder RJ, Shuman WP, McHugh JW, Marglin SI, Butler J. Preservation of normal lung regions in the adult respiratory distress syndrome: analysis by computed tomography. *JAMA* 1986;255:2463–2465.
6. Tremblay L, Valenza F, Ribeiro S, Li J, Slutsky AS. Injurious ventilatory strategies increase cytokines and c-fos mRNA expression in an isolated rat lung model. *J Clin Invest* 1997;99:944–952.
7. Vlahakis NE, Schroeder MA, Limper AH, Hubmayr RD. Stretch induces cytokine release by alveolar epithelial cells in vitro. *Am J Physiol Lung Cell Mol Physiol* 1999;277:L167–L173.
8. Liu M, Tanswell AK, Post M. Mechanical force-induced signal transduction in lung cells. *Am J Physiol Lung Cell Mol Physiol* 1999;277:L667–L683.
9. Prasad S, Thakur MK. Age-dependent effects of sodium butyrate and hydrocortisone on acetylation of high mobility group proteins of rat liver. *Biochem Int* 1988;16:375–382.
10. Wang H, Bloom O, Zhang M, Vishnubhakat JM, Ombrellino M, Che J, Frazier A, Yang H, Ivanova S, Borovikova L, *et al.* HMG-1 as a late mediator of endotoxin lethality in mice. *Science* 1999;285:248–251.
11. Ueno H, Matsuda T, Hashimoto S, Amaya F, Kitamura Y, Tanaka M, Kobayashi A, Maruyama I, Yamada S, Hasegawa N, *et al.* Contribution of high mobility group box protein in experimental and clinical acute lung injury. *Am J Respir Crit Care Med* 2004;170:1310–1316.
12. Abraham E, Arcaroli J, Carmody A, Wang H, Tracy KJ. HMG-1 as a mediator of acute lung inflammation. *J Immunol* 2000;165:2950–2954.
13. Scaffidi P, Misteli T, Bianchi ME. Release of chromatin protein HMGB1 by necrotic cells triggers inflammation. *Nature* 2002;418:191–195.
14. Yamamoto T, Kajikawa O, Martin TR, Sharar SR, Harlan JM, Winn RK. The role of leukocyte emigration and IL-8 on the development

of lipopolysaccharide-induced lung injury in rabbits. *J Immunol* 1998;161:5704–5709.
15. Yamada S, Inoue K, Yakabe K, Imaizumi H, Maruyama I. High mobility group protein 1 (HMGB1) quantified by ELISA with a monoclonal antibody that does not cross-react with HMGB2. *Clin Chem* 2003;49: 1535–1537.
16. Kotani M, Kotani T, Ishizaka A, Fujishima S, Koh H, Takasa S, Sawafuji M, Ikeda E, Moriyama K, Kotake Y, *et al.* Neutrophil depletion attenuates interleukin-8 production in mild-overstretch ventilated normal rabbit lung. *Crit Care Med* 2004;32:514–519.
17. Moriyama K, Ishizaka A, Nakamura M, Kubo H, Kotani T, Yamamoto S, Ogawa EN, Kajikawa O, Frevert CW, Kotake Y, *et al.* Enhancement of the endotoxin recognition pathway by ventilation with a large tidal volume in rabbits. *Am J Physiol Lung Cell Mol Physiol* 2004;286: L1114–L1121.
18. Bregeon F, Roch A, Delpierre S, Ghigo E, Autillo-Touati A, Kajikawa O, Martin TR, Pugin J, Portugal H, Auffray JP, *et al.* Conventional mechanical ventilation of healthy lungs induced pro-inflammatory cytokine gene transcription. *Respir Physiol Neurobiol* 2002;132:191–203.
19. Frank JA, Gutierrez JA, Jones KD, Allen L, Dobbs L, Matthay MA. Low tidal volume reduces epithelial and endothelial injury in acid-injured rat lungs. *Am J Respir Crit Care Med* 2002;165:242–249.
20. Kim JY, Park JS, Strassheim D, Douglas I, del Valle FD, Asehnoune K, Mitra S, Kwak SH, Yamada S, Maruyama I, *et al.* HMGB1 contributes to the development of acute lung injury after hemorrhage. *Am J Physiol Lung Cell Mol Physiol* 2005;288:L958–L965.
21. Hammerschmidt S, Kuhn H, Grasenack T, Gessner C, Wirtz H. Apoptosis and necrosis induced by cyclic mechanical stretching in alveolar type II cells. *Am J Respir Cell Mol Biol* 2004;30:396–402.
22. Degryse B, Bonaldi T, Scaffidi P, Müller S, Resnati M, Sanvito F, Arrigoni G, Bianchi ME. The high mobility group (HMG) boxes of the nuclear protein HMG1 induce chemotaxis and cytoskeleton reorganization in rat smooth muscle cells. *J Cell Biol* 2001;152:1197–1206.
23. Imanaka H, Shimaoka M, Matsuura N, Nishimura M, Ohta N, Kiyono H. Ventilator-induced lung injury is associated with neutrophil infiltration, macrophage activation, and TGF-beta 1 mRNA upregulation in rat lungs. *Anesth Analg* 2001;92:428–436.
24. Bonaldi T, Talamo F, Scaffidi P, Ferrera D, Porto A, Bachi A, Rubartelli A, Agresti A, Bianchi ME. Monocytic cells hyperacetylate chromatin protein HMGB1 to redirect it towards secretion. *EMBO J* 2003;22: 5551–5560.
25. Haslett C. Granulocyte apoptosis and its role in the resolution and control of lung inflammation. *Am J Respir Crit Care Med* 1999;160:S5–S11.
26. Miller EJ, Cohen AB, Nagao S, Griffith D, Maunder RJ, Martin TR, Weiner-Kronish JP, Sticherling M, Christophers E, Matthay MA. Elevated levels of NAP-1/interleukin-8 are present in the airspaces of patients with the adult respiratory distress syndrome and are associated with increased mortality. *Am Rev Respir Dis* 1992;146:427–432.
27. Donnelly SC, Strieter RM, Kunkel SL, Walz A, Robertson CR, Carter DC, Grant IS, Pollok AJ, Haslett C. Interleukin-8 and development of adult respiratory distress syndrome in at-risk patient groups. *Lancet* 1993;341:643–647.
28. Ricard JD, Dreyfuss D, Saumon G. Production of inflammatory cytokines in ventilator-induced lung injury: a reappraisal. *Am J Respir Crit Care Med* 2001;163:1176–1180.
29. Haitsma JJ, Uhlig S, Verbrugge SJ, Goggel R, Poelma DLH, Lachmann B. Injurious ventilation strategies cause systemic release of IL-6 and MIP-2 in rats in vivo. *Clin Physiol Funct Imaging* 2003;23:349–353.
30. Park JS, Arcaroli J, Yum HK, Yang H, Wang H, Yang KY, Choe KH, Strassheim D, Pitts TM, Tracey KJ, *et al.* Activation of gene expression in human neutrophils by high mobility group box 1 protein. *Am J Physiol Cell Physiol* 2003;284:C870–C879.
31. Andersson U, Wang H, Palmblad K, Aveberger A-C, Bloom O, Erlandsson-Harris H, Janson A, Kokkola R, Zhang M, Yang H, *et al.* High mobility group 1 protein (HMG-1) stimulates proinflammatory cytokine synthesis in human monocytes. *J Exp Med* 2000;192:565–570.
32. Fiuza C, Bustin M, Talwar S, Tropea M, Gerstenburger E, Shelhamer JH, Suffredini AF. Inflammation-promoting activity of HMGB-1 on human microvascular endothelial cells. *Blood* 2003;101:2652–2660.
33. Treutiger CJ, Mullins GE, Johansson ASM, Rouhiainen A, Rauvala HME, Erlandsson-Harris H, Andersson U, Yang H, Tracey KJ, Andersson J, *et al.* High mobility group 1 B-box mediates activation of human endothelium. *J Intern Med* 2003;254:375–385.
34. Verbrugge SJC, Uhlig S, Neggers SJCMM, Martin C, Held HD, Haitsma JJ, Lachmann B. Differential ventilation strategies affect lung function but do not increase tumor necrosis factor-α and prostacyclin production in lavaged rat lungs in vivo. *Anesthesiology* 1999;91:1834–1843.
35. Burke-Gaffney A, Hellewell PG. Tumor necrosis factor-α-induced ICAM-1 expression in human vascular endothelial and lung epithelial cells: modulation by tyrosine kinase inhibitors. *Br J Pharmacol* 1996; 119:1149–1158.
36. Woo CH, Lim JH, Kim JH. VCAM-1 upregulation via PKCδ-p38 kinase-linked cascade mediates the TNF-α-induced leukocyte adhesion and emigration in the lung airway epithelium. *Am J Physiol Lung Cell Mol Physiol* 2005;288:L307–L316.

J Anesth (2006) 20:208–214
DOI 10.1007/s00540-006-0411-z

Journal of
Anesthesia

Combined effects of propofol and mild hypothermia on cerebral metabolism and blood flow in rhesus monkey: a positron emission tomography study

TAKASHI OUCHI[1], RYOICHI OCHIAI[2], JUNZO TAKEDA[3], HIDEO TSUKADA[4], and TAKEHARU KAKIUCHI[4]

[1]Department of Anesthesiology, Tokyo Dental College, Ichikawa General Hospital, 5-11-13 Sugano, Ichikawa 272-8513, Japan
[2]Toho University School of Medicine, Tokyo, Japan
[3]Department of Anesthesiology, School of Medicine, Keio University, Tokyo, Japan
[4]Central Research Laboratory, Hamamatsu Photonics K.K., Hamamatsu, Japan

Abstract

Purpose. Propofol reduces the cerebral metabolic rate for oxygen ($CMRO_2$), regional $CMRO_2$ ($rCMRO_2$), cerebral blood flow (CBF), and regional CBF (rCBF), but maintains the coupling of cerebral metabolism and blood flow. Under mild to moderate hypothermia, the coupling is maintained, while rCBF is reduced, but no direct measurement of $rCMRO_2$ has yet been reported. This study aimed to evaluate the effects of propofol under normothermic and mild hypothermic temperatures upon $rCMRO_2$, rCBF, and their regional coupling, through direct measurement by positron emission tomography.

Methods. Rhesus monkeys were anesthetized with 65% nitrous oxide and propofol. Then rCBF and $rCMRO_2$ were measured under four sets of conditions: infusion of a low-propofol dose ($12\,mg \cdot kg^{-1} \cdot h^{-1}$) at normothermic temperatures (38°C), a high dose ($25\,mg \cdot kg^{-1} \cdot h^{-1}$) at normothermic temperatures, a low dose under mild hypothermia (35°C), and a high dose under mild hypothermia. The ratio of $rCBF/rCMRO_2$ was calculated from these data.

Results. Reductions in $CMRO_2$ and $rCMRO_2$ in most regions were associated with two factors: the higher propofol dose and the induction of hypothermia, but there was no interaction between these factors. Concerning blood flow, no significant reduction was observed, except for CBF by the induction of hypothermia. The ratio of $rCBF/rCMRO_2$ was constant in this study setting.

Conclusion. During propofol anesthesia, it is possible to reduce cerebral metabolism throughout the entire brain as well as in any brain region by increasing the propofol dose or inducing hypothermia. The concurrent use of these two interventions has an additive effect on metabolism, and can be considered as safe, as their combination does not impair the coupling of cerebral metabolism and blood flow.

Key words Propofol · Mild hypothermia · Cerebral metabolism · Cerebral blood flow · Coupling of cerebral metabolism and blood flow

Address correspondence to: T. Ouchi
Received: August 4, 2005 / Accepted: April 11, 2006

Introduction

Most intravenous anesthetics have an inhibitory effect on the central nervous system by suppressing cerebral electrophysiologic function [1], which results in a reduction in cerebral metabolism accompanied by decreased cerebral blood flow (CBF) [1]. In humans, administration of propofol results in reductions in the cerebral metabolic rate of oxygen ($CMRO_2$) [2,3], regional $CMRO_2$ ($rCMRO_2$) [4], CBF [2,3,5], and regional CBF (rCBF) [6], but the coupling of cerebral metabolism and blood flow is maintained at anesthetic doses [3]. In animal studies, propofol also decreases $rCMRO_2$ [7] and rCBF [7–9], but does not inhibit their coupling [7]. It has been suggested that propofol preserves both cerebral autoregulation [10–12] and carbon dioxide responsiveness [11–14].

Hypothermia reduces $CMRO_2$ [1,15,16] by suppressing cerebral electrophysiologic activity and decreasing cerebral metabolic activity, thereby working to maintain cellular homeostasis [1]. This reduction makes it useful for protecting the brain during cardiovascular surgery and as a therapeutic measure in patients with cerebral ischemia. Under mild to moderate hypothermia, the coupling of cerebral metabolism and blood flow is maintained [17,18], while rCBF is reduced [17]. However, to the best of our knowledge, no direct measurement of hypothermic $rCMRO_2$ has yet been reported.

The mechanisms by which intravenous anesthetics and hypothermia inhibit central nervous system activity are known to be different [1]. But the nature and extent of the interactions between these two interventions and those of the coupling of cerebral metabolism and blood flow remain poorly understood. We believe that elucidating the effect of the interaction between intravenous anesthetics and hypothermia upon $rCMRO_2$ and the coupling of cerebral metabolism and blood flow will lead us to a better understanding of

the safe management of general anesthesia under hypothermia.

Positron emission tomography (PET) is a nuclear imaging technique, used to measure gamma ray activity from chemical compounds labeled with positron-emitting isotopes. This technique enables the direct and noninvasive measurement of the regional distribution and kinetics of the labeled compounds in the body and brain, and the very short half-lives of the labeled isotopes allows for repeated measurements at brief intervals. These characteristics seemed to make PET the ideal method for this study, which required multiple measurements of $rCMRO_2$ and rCBF.

The aim of this study was to evaluate the effects of propofol under varying temperatures upon regional cerebral metabolism and blood flow, and their regional coupling in particular, through the direct measurement of $rCMRO_2$ and rCBF by PET in rhesus monkeys.

Materials and methods

The protocol of this experiment was approved by the Animal Ethics Committee, Central Research Laboratory, Hamamatsu Photonics.

General procedure

Three adult rhesus monkeys (*Macaca mulatta*), weighing 4.2–6.4 kg, were studied; in the first one, experiments were done three times, in the second, one time, and in the third, two times. These experiments were done on separate days at least 4 weeks apart. The animals were maintained and handled in accordance with United States National Institutes of Health recommendations on animal care and the guidelines of the Central Research Laboratory, Hamamatsu Photonics.

The animals were fasted but allowed free access to water for at least 12 h before the induction of anesthesia; 0.02–0.05 $mg \cdot kg^{-1}$ of atropine sulfate was given intramuscularly as premedication.

General anesthesia was induced by the intramuscular injection of 7.5–10 $mg \cdot kg^{-1}$ of ketamine hydrochloride. The animals were intubated using an endotracheal tube equipped with a cuff (Lo-Pro; Mallinckrodt, Athlone, Ireland), and mechanically ventilated to strictly maintain normocapnia (arterial partial pressure of CO_2 [Pa_{CO_2}], 39–41 mmHg).

During surgical procedures, anesthesia was maintained with 65% nitrous oxide (N_2O) and 2% sevoflurane. A cephalic vein was cannulated with a 24-G catheter, and lactated Ringer's solution was infused at 4 to 5 $ml \cdot kg^{-1} \cdot h^{-1}$. A femoral artery was cannulated with a 20-G catheter, and an intravascular probe, used for monitoring continuous blood gas (Paratrend 7; Diametrics Medical, St. Paul, MN, USA), was inserted into the artery through this catheter. After these procedures, sevoflurane was terminated, and anesthesia was maintained with 65% N_2O and propofol. An initial 25-mg bolus of propofol (3.9–6.0 $mg \cdot kg^{-1}$) was administered, followed by continuous infusion of propofol at 12 $mg \cdot kg^{-1} \cdot h^{-1}$. Vecuronium bromide was injected intermittently.

Arterial blood pressure, electrocardiograph, and rectal temperature were monitored throughout the study (Nihon Kohden, Tokyo, Japan). Pa_{CO_2} and Pa_{O_2} were monitored using a continuous blood gas monitoring system, and endtidal concentrations of inhalation anesthetics and CO_2 were monitored using an anesthesia machine (Cato, Dräger, Germany).

After the surgical procedures, the animal was kept in a supine position and its head was immobilized using an acrylic resin restraint developed by the study team. The orbito-meatal (OM) line was adjusted to the zero point of the PET scanner; 30-min-transmission scan data were collected before the first measurement.

After the measurements were completed, the animal was extubated and treated, following the animal care guidelines, after recovery from anesthesia.

PET scan

Data were collected using a high-resolution animal PET scanner (SHR-7700; Hamamatsu Photonics, Hamamatsu, Japan), with transaxial resolution of 2.6 mm full width at half maximum in the center of the scan field, and a center-to-center distance of 3.6 mm [19]. The PET camera allowed 16 to 17 slices for imaging to be recorded simultaneously.

Measurements

In this study, ^{15}O (half-life, 2.04 min) was used as the positron-emitting isotope.

For the measurement of rCBF and $rCMRO_2$, 2.3 $GBq \cdot min^{-1}$ of ^{15}O-CO_2 gas was used as a tracer to measure rCBF, and 2.0 $GBq \cdot min^{-1}$ of ^{15}O-O_2 gas was used to measure $rCMRO_2$. Each gas was continuously supplied through a gas administration system (Sumitomo Heavy Industry, Tokyo, Japan), and mixed into the oxygen and nitrous oxide in the anesthesia circuit. After the activity of gamma rays radiating from the cranium reached equilibrium, a 6-min scan was initiated. At the end of the scan, the delivery of gas was terminated, and an interval of more than 15 min was allowed before the next measurement to permit the isotope radioactivity to decay.

For the calculation of rCBF and $rCMRO_2$, the partition coefficient and hematocrit ratio were set at 0.95 and 0.85, respectively [19].

Conditions

In each experiment, rCBF and $rCMRO_2$ were measured under the following four sets of conditions, in the following order, at least 30 min apart.

Low-dose/Normo. Infusion of propofol given at 12 $mg \cdot kg^{-1} \cdot h^{-1}$ at normothermic temperatures (rectal temperature, ~38°C).

High-dose/Normo. Infusion of propofol given at 25 $mg \cdot kg^{-1} \cdot h^{-1}$ at normothermic temperatures.

Low-dose/Hypo. Infusion of propofol given at 12 $mg \cdot kg^{-1} \cdot h^{-1}$ under mild hypothermia (rectal temperature, ~35°C).

High-dose/Hypo. Infusion of propofol given at 25 $mg \cdot kg^{-1} \cdot h^{-1}$ under mild hypothermia.

In this study, we regarded low-dose/normo as the control condition; a low dose of anesthetic was necessary, as surgically treated animals require some form of sedation. During the experiments, blood pressure was maintained at the level of low dose/normo by the continuous infusion of angiotensin II (AT II; Sigma Chemical, St. Louis, MO, USA), as necessary.

The normal body temperature of the rhesus monkey is 38°C; this temperature was regarded as normothermia, and 35°C as hypothermia. Body temperature was maintained using a blanket, an electric warming mat, and disposable pocket warmers. Hypothermia was maintained by ventilating the air with a fan.

Statistical analysis

Areas in the frontal cortex, temporal cortex, parietal cortex, occipital cortex, cerebellar cortex, thalamus, and white matter were selected as regions of interest (ROI). The areas of these ROIs were chosen (or sectioned) in reference to magnetic resonance images ([MRI]; MRT-50A/II; Toshiba, Tokyo, Japan), and the stereotaxic coordination of PET and MRI was adjusted based on the OM reference line.

Datum for whole brain was calculated as the average of data from all slices, and datum for each ROI was calculated as that of two data from different slices. The ratio of $rCBF/rCMRO_2$ was calculated using the rCBF and $rCMRO_2$ data.

Two-way analysis of variance was used for statistical comparisons. The Student Newman-Keuls test was used as a post hoc test. In this study, $P < 0.05$ was considered to indicate statistical significance.

Results

Physiological variables (Table 1)

Mean arterial pressure (MAP) and heart rate (HR) varied in each subject, but in most cases, MAP was

Table 1. Physiological variables

		Normothermia		Hypothermia	
Experiment no.	Parameters	Low-dose propofol	High-dose propofol	Low-dose propofol	High-dose propofol
1	MAP/HR	130/160	130/150	130/130	125/130
	Pa_{CO_2}/RT	40.6/38.3	39.7/37.8	40.0/35.0	39.9/35.0
	AT II	0	13.0	5.0	15.0
2	MAP/HR	140/125	135/145	160/115	130/105
	Pa_{CO_2}/RT	39.6/37.5	40.4/37.8	40.5/34.9	39.9/35.0
	AT II	0	6.0	4.0	8.0
3	MAP/HR	125/150	135/145	135/120	125/130
	Pa_{CO_2}/RT	39.6/38.3	39.9/38.1	40.1/35.1	40.0/35.0
	AT II	0	2.5	0.5	1.5
4	MAP/HR	75/140	70/140	100/100	75/100
	Pa_{CO_2}/RT	40.0/38.1	40.2/38.1	39.6/34.8	39.7/34.9
	AT II	0	0.8	0	0.8
5	MAP/HR	75/120	70/120	80/100	70/90
	Pa_{CO_2}/RT	40.1/38.1	39.9/38.3	40.4/35.4	39.5/35.3
	AT II	0	0	0	0
6	MAP/HR	80/110	70/100	85/80	70/80
	Pa_{CO_2}/RT	39.7/38.2	39.7/38.4	40.1/35.1	40.2/35.3
	AT II	0	0	0.4	0.6

The condition of "hypothermia" was a significantly affecting factor for HR ($P = 0.003$)
Under the condition of "normothermia", body temperature was maintained at approximately 38°C, and under the condition of "hypothermia" body temperature was maintained at approximately 35°C. Under the condition of "Low-dose propofol", 12 $mg \cdot kg^{-1} \cdot h^{-1}$ of propofol was administered, and under the condition of "high-dose propofol", 25 $mg \cdot kg^{-1} \cdot h^{-1}$ of propofol was administered
MAP, mean arterial blood pressure (mmHg); HR, heart rate (bpm); Pa_{CO_2}, arterial partial pressure of carbon dioxide (mmHg); RT, rectal temperature (°C); AT II, dose of angiotensin II ($ng \cdot kg^{-1} \cdot min^{-1}$)

maintained at the same level as in low-dose/normo, the control value in this study. The maximum dose of AT II required to maintain MAP was 15 ng·kg^{-1}·h^{-1}. We did not attempt to maintain HR, which showed a significant reduction on the induction of mild hypothermia (P = 0.0026), but not on the increase of the propofol dose from 12 mg·kg^{-1}·h^{-1} to 25 mg·kg^{-1}·h^{-1} (P = 0.8752). In all cases, the rectal temperature of the subjects was maintained at approximately 38°C in the normothermic conditions, and at approximately 35°C in the hypothermic conditions. Pa_{CO_2} was maintained between 39 and 41 mmHg throughout all of the studies.

CBF and $CMRO_2$ in whole brain (Table 2)

$CMRO_2$ showed a significant reduction on the increase of the propofol dose from 12 mg·kg^{-1}·h^{-1} to 25 mg·kg^{-1}·h^{-1}, as well as on the induction of hypothermia. CBF significantly decreased under hypothermia. With the increased propofol dose, CBF decreased by 22% under normothermia and by 15% under hypothermia, but these changes were not statistically significant. There were no significant changes in $CBF/CMRO_2$.

Values of rCBF and $rCMRO_2$ (Table 3)

The $rCMRO_2$ values in all ROIs showed significant reductions on the induction of mild hypothermia. In all ROIs, except for the occipital and cerebellar cortexes, $rCMRO_2$ decreased significantly under the higher propofol dose, but rCBF was not significantly reduced by either the increased propofol dose or by hypothermia, the only exception being the frontal cortex, in which rCBF was reduced at the higher propofol dose. There was no significant change in regional $CBF/CMRO_2$ in any ROI, as was the case in the whole brain.

Discussion

The main findings of this study were: (1) reductions in whole brain $CMRO_2$ and $rCMRO_2$ in most ROIs were associated with two factors: the higher propofol dose and the induction of hypothermia, but there was no interaction between these two factors; (2) whole brain CBF decreased under hypothermia, but not at the higher propofol dose in this study setting; (3) no rCBF showed significant reduction under either higher propofol dose (except for that in the frontal cortex) or mild hypothermia; and, (4) $CBF/CMRO_2$ in both the whole brain and in all ROIs was unaffected by these factors.

In this study, $CMRO_2$ in the whole brain decreased in response to two factors, higher propofol dose and mild hypothermia, which was in line with findings from

Table 2. CBF and $CMRO_2$ in whole brain

	Normothermia		Hypothermia		*P* value		
	Low-dose propofol	High-dose propofol	Low-dose propofol	High-dose propofol	Propofol dose	Body temperature	Interaction
CBF	23.6 ± 7.1	18.5 ± 3.4	18.0 ± 4.7	15.6 ± 3.8	0.08	0.048*	0.51
$CMRO_2$	2.3 ± 0.3	1.8 ± 0.3	1.7 ± 0.4	1.4 ± 0.3	0.01*	0.003*	0.43
$CBF/CMRO_2$	10.4 ± 2.7	10.6 ± 1.9	10.6 ± 2.3	10.9 ± 1.9	0.77	0.80	0.95

*Factor that significantly affected CBF or $CMRO_2$ ($P < 0.05$)
Data values are presented as means ± SD
Under the condition of "normothermia", body temperature was approximately 38°C and under the condition of "hypothermia", it was approximately 35°C. Under the condition of "low-dose propofol", 12 mg·kg^{-1}·h^{-1} of propofol was administered, and under the condition of "high-dose propofol", 25 mg·kg^{-1}·h^{-1} of propofol was administered
CBF, cerebral blood flow (ml·min^{-1}·100 g tissue^{-1}); $CMRO_2$, cerebral metabolic rate of oxygen (ml·min^{-1}·100 g tissue^{-1}); interaction, interaction between the two factors of propofol dose and body temperature

Table 3. Values of rCBF and $rCMRO_2$

Region of interest	Parameters	Normothermia		Hypothermia		*P* value		
		Low-dose propofol	High-dose propofol	Low-dose propofol	High-dose propofol	Propofol dose	Body temperature	Interaction
Frontal cortex	rCBF	22.6 ± 7.4	16.7 ± 2.8	17.6 ± 4.6	14.5 ± 3.6	0.03*	0.09	0.50
	$rCMRO_2$	2.1 ± 0.4	1.5 ± 0.4	1.6 ± 0.5	1.3 ± 0.4	0.01*	0.048*	0.63
	$rCBF/rCMRO_2$	11.0 ± 4.1	11.4 ± 3.5	11.1 ± 3.5	11.9 ± 4.1	0.74	0.84	0.89
Temporal cortex	rCBF	25.5 ± 9.8	18.8 ± 3.8	18.9 ± 6.0	15.9 ± 5.2	0.08	0.09	0.49
	$rCMRO_2$	2.3 ± 0.5	1.7 ± 0.4	1.7 ± 0.5	1.4 ± 0.3	0.02*	0.02*	0.55
	$rCBF/rCMRO_2$	11.1 ± 3.4	11.0 ± 2.0	10.8 ± 2.0	11.0 ± 1.8	0.96	0.90	0.84
Parietal cortex	rCBF	22.1 ± 6.9	17.3 ± 3.4	17.2 ± 4.6	15.1 ± 3.7	0.10	0.09	0.50
	$rCMRO_2$	2.0 ± 0.4	1.5 ± 0.4	1.5 ± 0.5	1.3 ± 0.3	0.04*	0.02*	0.39
	$rCBF/rCMRO_2$	10.9 ± 3.0	11.7 ± 3.1	12.3 ± 3.9	12.3 ± 3.3	0.76	0.48	0.77
Occipital cortex	rCBF	22.0 ± 6.5	19.5 ± 5.1	17.8 ± 5.3	16.6 ± 5.0	0.43	0.13	0.77
	$rCMRO_2$	2.1 ± 0.4	1.7 ± 0.4	1.4 ± 0.2	1.4 ± 0.3	0.12	0.002*	0.21
	$rCBF/rCMRO_2$	10.5 ± 2.3	11.6 ± 2.5	12.4 ± 3.0	12.0 ± 2.3	0.72	0.27	0.47
Cerebellar cortex	rCBF	21.1 ± 5.7	18.7 ± 4.9	17.4 ± 5.3	15.8 ± 4.9	0.36	0.13	0.85
	$rCMRO_2$	2.1 ± 0.4	1.7 ± 0.3	1.5 ± 0.3	1.5 ± 0.3	0.16	0.002*	0.12
	$rCBF/rCMRO_2$	9.8 ± 2.1	10.7 ± 2.2	12.0 ± 3.5	10.5 ± 1.7	0.78	0.33	0.25
Thalamus	rCBF	24.1 ± 6.3	19.7 ± 5.7	18.9 ± 5.9	16.1 ± 4.6	0.13	0.07	0.74
	$rCMRO_2$	2.4 ± 0.3	2.0 ± 0.4	2.0 ± 0.6	1.6 ± 0.4	0.02*	0.03*	0.88
	$rCBF/rCMRO_2$	9.9 ± 2.6	10.1 ± 2.0	9.5 ± 2.4	10.3 ± 1.5	0.58	0.91	0.77
White matter	rCBF	24.5 ± 9.6	17.6 ± 3.5	17.5 ± 5.0	14.9 ± 3.7	0.06	0.06	0.40
	$rCMRO_2$	2.2 ± 0.4	1.8 ± 0.4	1.7 ± 0.4	1.5 ± 0.3	0.02*	0.01*	0.50
	$rCBF/rCMRO_2$	10.7 ± 3.6	10.0 ± 2.1	10.1 ± 2.1	10.1 ± 1.9	0.78	0.75	0.74

*Factor that significantly affected rCBF or $rCMRO_2$ ($P < 0.05$)
Data values are presented as means ± SD
Under the condition of "normothermia", body temperature was approximately 38°C and under the condition of "hypothermia", it was approximately 35°C. Under the condition of "low-dose propofol", 12 mg·kg^{-1}·h^{-1} of propofol was administered, and under the condition of "high-dose propofol", 25 mg·kg^{-1}·h^{-1} of propofol was administered
rCBF, regional cerebral blood flow (ml·min^{-1}·100 g tissue^{-1}); $rCMRO_2$, regional cerebral metabolic rate of oxygen (ml·min^{-1}·100 g tissue^{-1}); interaction, interaction between the two factors propofol dose and body temperature

numerous previous reports [2,3,15–18,20,21]. The $rCMRO_2$ values in all ROIs showed significant reductions under hypothermia, as expected [1]. The increased propofol dose was associated with significant reductions in $rCMRO_2$ in all ROIs except for the occipital and cerebellar cortexes. This exception arose from the results that $rCMRO_2$ in these two ROIs was not diminished by increasing propofol dose under mild hypothermia. It might be suggested that even mild hypothermia suppresses not only the energy requirement for the maintenance of cellular homeostasis but also a great amount of the requirement for electrophysiologic activity, so that increasing the propofol dose has little effect on $rCMRO_2$ in these ROIs.

One of our new findings is that there was no interaction between the effects of increased propofol dose and mild hypothermia on either $CMRO_2$ or $rCMRO_2$ in most of the ROIs, suggesting that the suppressive effect of these two factors on both the entire brain and specific brain regions under our experimental conditions was neither synergistic nor antagonistic, but simply additive. It is known that hypothermia causes reductions in cerebral metabolism by suppressing electrophysiologic activity and metabolic activity in the maintenance of cellular homeostasis, while propofol causes similar reductions by its inhibition of electrophysiologic activity [1]. It can be seen that electrophysiologic function is well maintained under mild hypothermia, so additional propofol may further suppress this function.

In this study, whole brain CBF was reduced on the induction of mild hypothermia, as has been reported elsewhere [15–17,22]. The higher propofol dose was associated with a 22% reduction of CBF under normothermia and a 15% reduction under hypothermia; however, these decreases were not statistically significant, and such findings are different from those reported in previous studies [2,3,5,20,21]. The rCBF did not show significant reductions in any ROIs either at the higher propofol dose or under hypothermia, with only one exception—the frontal cortex. It can be considered that the wide variation of rCBF and CBF values made it difficult to define the statistical significance of these decreases in rCBF and CBF.

In order to evaluate the coupling of cerebral metabolism and blood flow, CBF must be observed under stable cardiovascular conditions, while the cerebral metabolism is changed. But this method of observation could not be done in our study design; thus, we calculated $CBF/CMRO_2$ and used this ratio as the index of the coupling. In both the whole brain and specific brain regions, this ratio showed a wide range of variation in each subject, but did not show specific, statistically significant changes. We concluded that the coupling of cerebral metabolism and blood flow was not affected by either an increased dose of propofol or the induction of mild hypothermia. It has been reported in studies using the Kety-Schmidt method [3] or PET scans [7] that this coupling is maintained under propofol anesthesia. It has also been shown in studies using the colored microsphere method [17] or PET scans [18] that the coupling is maintained under mild to moderate hypothermia. Our findings are consistent with these previous studies.

Six experiments, using the PET technique, were performed on three rhesus monkeys in our study, which was rather small in number. But it should be noted that this technique is an expensive method because of the requirement for a cyclotron, and also it is difficult to keep a large number of primates in one facility. In spite of the limitation in sample numbers, using the PET technique in primates brings us many important findings, which cannot be obtained by ordinary methods, or from other species.

We induced anesthesia with ketamine hydrochloride, and it is well known that this agent increases $CMRO_2$, followed by an increase in CBF [1]. But as we found that the blood concentration of ketamine could not be detected at the time of the first measurement of PET in our previous study [23], we regard the influence of ketamine as negligible. We maintained anesthesia with sevoflurane during surgical procedures. In another previous study, we found that sevoflurane decreased $rCMRO_2$, but did not change rCBF or affect coupling [24]. However, in the present study, the endtidal concentration of sevoflurane was zero at least 30 min before the first PET measurement, and we have also regarded the influence of sevoflurane as negligible.

We used N_2O throughout this experiment, because analgesia was necessary to minimize the wound pain after the surgery. The lack of pharmacokinetic information for the rhesus monkey precluded the use of intravenous analgesics, including opiates, as it would have been impossible to maintain stable effect site concentrations throughout the study. It has been shown that N_2O increases CBF [25–28], and its effect plateaus at an inhalation concentration of approximately 30% [28]. But it has also been reported that the inhalation of 20% N_2O does not affect the coupling of cerebral metabolism and blood flow [27]. Given these data, it was our belief that the effects of an increased propofol dose and hypothermia on rCBF and $rCMRO_2$ could be evaluated, as long as the concentration of N_2O was kept constant throughout the study.

In the study reported by Enlund et al. [7], the basic dose of propofol in the rhesus monkey was $6\,mg \cdot kg^{-1} \cdot h^{-1}$, while our low-dose control was $12\,mg \cdot kg^{-1} \cdot h^{-1}$. In our pilot study, we observed changes in blood pressure and heart rate in response to weak auditory stimulation, at propofol doses of less than $10\,mg \cdot kg^{-1} \cdot h^{-1}$, which led us to conclude that $10\,mg \cdot kg^{-1} \cdot h^{-1}$ was the minimal anesthetic dose. Target-